

Distribution Agreement

In presenting this thesis as a partial fulfillment of the requirements for a degree from Emory University, I hereby grant to Emory University and its agents the non-exclusive license to archive, make accessible, and display my thesis in whole or in part in all forms of media, now or hereafter now, including display on the World Wide Web. I understand that I may select some access restrictions as part of the online submission of this thesis. I retain all ownership rights to the copyright of the thesis. I also retain the right to use in future works (such as articles or books) all or part of this thesis.

Sneh Patel

April 10th, 2023

Brain GALT restoration by intrathecal injection of scAAV9-hGALT enables partial metabolic correction in adolescent GALT-null rats

by

Sneh Patel

Dr. Judith Fridovich-Keil
Advisor

Neuroscience and Behavioral Biology

Dr. Judith Fridovich-Keil
Advisor

Dr. Leah Roesch
Committee Member

Dr. Patrick Cafferty
Committee Member

2023

Brain GALT restoration by intrathecal injection of scAAV9-hGALT enables partial metabolic correction in adolescent GALT-null rats

by

Sneh Patel

Dr. Judith Fridovich-Keil
Advisor

An abstract of
a thesis submitted to the Faculty of Emory College of Arts and Sciences
of Emory University in partial fulfillment
of the requirements of the degree of
Bachelor of Science with Honors

Neuroscience and Behavioral Biology

2023

Abstract

Classic Galactosemia (CG) is a potentially lethal autosomal recessive disorder caused by a severe deficiency of galactose-1-phosphate uridylyl transferase (GALT). Following galactose exposure, newborns with CG develop feeding difficulties, cataracts, failure to thrive, hepatocellular damage, hypotonia, renal tubular disease, and *E. coli* sepsis, which can lead to neonatal death. The current therapeutic standard of care for galactosemic patients is a galactose-restricted diet which is effective in nullifying acute neonatal complications but is inadequate in preventing long-term complications such as cognitive deficits, problems with speech, fine motor skills deficits, persistent cataracts, and primary ovarian insufficiency in young women. *GALT* gene therapy is currently being investigated as a potential treatment to directly restore GALT activity. The overarching goal of the study is to test the efficacy of scAAV9-mediated hGALT replacement administered intrathecally in adolescent GALT-null rats. GALT enzymes assays confirmed successful hGALT transduction in the brains of GALT-null rats that persisted for at least four months with fairly high tissue specificity. Previous studies have suggested accumulation of galactose metabolites from the Leloir pathway may be the root cause of some of the adverse phenotypes associated with CG. Galactitol responded well at 30 days after treatment in both brain and plasma. However, other metabolic abnormalities were not significantly reduced at the three timepoints in the study. The lack of significant metabolic efficacy could be attributed to insufficient GALT restoration in the brain and/or the inability of the brain to metabolize galactose sufficiently to “scrub the blood”. Although our current findings are inconclusive, future research, for example with higher doses or altered virus with improved access to the brain could potentially provide greater metabolic impact. The results reported here represent a major conceptual step in the direction of developing an effective gene therapy treatment option for adolescent patients with CG.

Brain GALT restoration by intrathecal injection of scAAV9-hGALT enables partial metabolic correction in adolescent GALT-null rats

by

Sneh Patel

Dr. Judith Fridovich-Keil
Advisor

A thesis submitted to the Faculty of Emory College of Arts and Sciences
of Emory University in partial fulfillment
of the requirements of the degree of
Bachelor of Science with Honors

Neuroscience and Behavioral Biology

2023

Acknowledgements

I would like to thank Dr. Fridovich-Keil for accepting me into her lab and supporting me over the last four years on various projects, including this one. I am grateful for all the time she has dedicated towards my success. Her mentorship has been invaluable throughout my undergraduate career, and I will forever be indebted to her for providing me with the resources to conduct research in her lab.

I would also like to thank Dr. Shauna Rasmussen for mentoring me on practical and theoretical skills in the lab. Dr. Rasmussen has played a monumental role in this project by performing all tissue collections and helping with metabolite extractions. I could not have completed this project with her constant support. Additionally, I would like to thank Lingyuan Wu for teaching me her methods for performing enzyme assays and troubleshooting problems as they arose.

Finally, I would like to thank Dr. Anthony Donsante for performing all of the intrathecal injections for this project. I would also like to thank all members of the Fridovich-Keil lab, particularly Aarjav Pandya and Aaron Wozniak, for supporting me through various stages of the project. I could not have completed this project without their help and countless hours spent in executing different experiments of the project.

Table of Contents

Chapter 1: Background and Introduction.....	1
<i>Description of Classic Galactosemia and Patient Experience</i>	1
<i>The Leloir Pathway of Galactose Metabolism</i>	3
<i>Current Treatment and Gene-Based Therapeutic Approaches</i>	4
<i>Adeno-Associated Virus (AAV)-Mediated Therapy</i>	6
<i>The CG Rat Model</i>	8
<i>Neonatal AAV-mediated GALT Restoration Offers Metabolic and Phenotypic Partial Rescue</i>	10
<i>Significance of the study</i>	10
Chapter 2: GALT restoration in brain following adolescent intrathecal administration of scAAV9-hGALT.....	13
<i>Introduction</i>	13
<i>Materials and Methods</i>	13
<i>Results</i>	21
<i>Discussion</i>	28
Chapter 3: Metabolic efficacy in brain and plasma following adolescent intrathecal administration of scAAV9-hGALT	30
<i>Introduction</i>	30
<i>Materials and Methods</i>	30
<i>Results</i>	37
<i>Discussion</i>	59
Chapter 4: Discussion, Limitations, and Future Directions	61
References.....	65

Tables

1. Properties of AAV serotypes	8
2. Cohort sizes of the treatment groups in the experiment	11
3. Amount of protein used for the GALT assays by genotype and tissue-type	17
4. Brain samples analyzed in Chapter 2	20
5. Liver samples analyzed in Chapter 2	20
6. Dilutions used for brain metabolites by genotype and time post-treatment	32
7. Dilutions used for plasma metabolites by genotype and time post-treatment	32
8. Brain samples analyzed in Chapter 3	35
9. Plasma samples analyzed in Chapter 3	36

Figures

1. Leloir pathway of galactose metabolism	4
2. The <i>Galt</i> ^{M3} mutation created by CRISPR-Cas9 gene editing	9
3. Image of intrathecal injection into a rat by Dr. Anthony Donsante	15
4. Chromatogram of a brain sample processed on a PA10 column	19
5. Brain GALT activity by treatment group one month after injection	22
6. Brain GALT activity by treatment group two months after injection	22
7. Brain GALT activity by treatment group four months after injection	23
8. Brain GALT activity over time in WT rats treated with PBS.....	24
9. Brain GALT activity over time in M3/M3 rats treated with PBS.....	24
10. Brain GALT activity over time in M3/M3 rats treated with scAAV9.CBh.HA-hGALT.....	25
11. Brain GALT activity over time by treatment group and time post-injection	25
12. Liver GALT activity by treatment group one month after injection	26
13. Liver GALT activity by treatment group two months after injection.....	26
14. Liver GALT activity by treatment group four months after injection	27
15. Muscle GALT activity by treatment group one month after injection	27
16. Chromatogram of a brain sample processed on an MA1 column.....	34
17. Brain galactitol levels by treatment group one month after injection.....	38
18. Brain galactitol levels by treatment group two months after injection	38
19. Brain galactitol levels by treatment group four months after injection	39
20. Brain galactose levels by treatment group one month after injection.....	39
21. Brain galactose levels by treatment group two months after injection	40
22. Brain galactose levels by treatment group four months after injection	40
23. Brain gal1P levels by treatment group one month after injection	41
24. Brain gal1P levels by treatment group two months after injection.....	41
25. Brain gal1P levels by treatment group four months after injection	42
26. Brain galactitol levels over time in WT rats treated with PBS	42
27. Brain galactitol levels over time in M3/M3 rats treated with PBS	43
28. Brain galactitol levels over time in M3/M3 rats treated with scAAV9.CBh.HA-hGALT	43
29. Brain galactose levels over time in WT rats treated with PBS	44

30. Brain galactose levels over time in M3/M3 rats treated with PBS	44
31. Brain galactose levels over time in M3/M3 rats treated with scAAV9.CBh.HA-hGALT	45
32. Brain gal1P levels over time in WT rats treated with PBS	45
33. Brain gal1P levels over time in M3/M3 rats treated with PBS	46
34. Brain gal1P levels over time in M3/M3 rats treated with scAAV9.CBh.HA-hGALT	46
35. Brain galactitol levels over time by treatment group and time post-injection	47
36. Brain galactose levels over time by treatment group and time post-injection	47
37. Brain gal1P levels over time by treatment group and time post-injection	48
38. Plasma galactitol levels by treatment group one month after injection	49
39. Plasma galactose levels by treatment group one month after injection	50
40. Plasma galactitol levels by treatment group two months after injection	50
41. Plasma galactose levels by treatment group two months after injection	51
42. Plasma galactitol levels by treatment group four months after injection	51
43. Plasma galactose levels by treatment group four months after injection	52
44. Plasma galactitol levels over time in WT rats treated with PBS	52
45. Plasma galactose levels over time in WT rats treated with PBS	53
46. Plasma galactitol levels over time in M3/M3 rats treated with PBS	53
47. Plasma galactose levels over time in M3/M3 rats treated with PBS	54
48. Plasma galactitol levels over time in M3/M3 rats treated with scAAV9.CBh.HA-hGALT ..	54
49. Plasma galactose levels over time in M3/M3 rats treated with scAAV9.CBh.HA-hGALT ..	55
50. Plasma galactitol levels over time by treatment group and time post-injection	55
51. Plasma galactose levels over time by treatment group and time post-injection	56
52. Relationship between brain galactitol levels and brain GALT activity	57
53. Relationship between brain galactose levels and brain GALT activity	57
54. Relationship between brain gal1P levels and brain GALT activity	58
55. Relationship between plasma galactitol levels and brain GALT activity	58
56. Relationship between plasma galactose levels and brain GALT activity	59

Chapter 1: Background and Introduction

Description of Classic Galactosemia and Patient Experience

Classic Galactosemia (CG) is a potentially lethal autosomal recessive disorder caused by a severe deficiency of the second enzyme of the Leloir pathway of galactose metabolism, galactose-1-phosphate uridylyl transferase (GALT) [1]. The human *GALT* gene, encoded on chr.9p13, includes 11 exons and spans just over 4 kilobases [2]. CG shows significant allelic heterogeneity, and the most reported mutational sites include Q188R, S135L, K285N, and L195P [3]. The most prevalent mutation in CG patients of northern European ancestry is Q188R accounting for 60-70% of the mutant *GALT* alleles identified in Caucasians [4]. This missense substitution results from an A to G transition in exon 6 that converts a glutamine codon near the catalytic site into an arginine codon [2]. The S135L mutation is most frequently observed in patients of African ancestry and accounts for 50% of the mutant *GALT* alleles in this population [3]. This substitution mutation has greater residual catalytic activity in hepatocytes and typically presents as a milder phenotype [2]. The K285N mutation is mostly found in the eastern European population and the L195P mutation is observed in less than 5% of CG alleles [3]. CG occurs with a prevalence of 1/40,000 to 1/60,000 infants in the United States [5]. CG is diagnosed through newborn screening (NBS) by detection of elevated erythrocyte galactose-1-phosphate (Gal-1P) concentration, reduced erythrocyte GALT activity, and/or biallelic pathogenic variants in *GALT* [1]. Affected infants are shifted from milk to a low-galactose soy or elemental formula immediately following an out-of-range NBS result.

Following exposure to breast milk or cow's milk-based formula, both of which contain high levels of galactose in the form of lactose, newborns with CG develop feeding difficulties, cataracts, failure to thrive, hepatocellular damage, hypotonia, renal tubular disease, and *E. coli*

sepsis, which can lead to neonatal death [6]. Without intervention, affected infants often die in the neonatal period [7]. Early detection by NBS, coupled with early and lifelong dietary restriction of galactose, prevents the acute and potentially lethal symptoms of CG. However, many affected children grow to experience central nervous system problems and long-term developmental and other complications such as speech impairment, motor or neurological disabilities, cognitive, and behavioral challenges in patients of both sexes, and primary ovarian insufficiency (POI) in girls and women [1]. The long-term outcomes in affected individuals show incomplete penetrance and variable expressivity, and while several studies have attempted to address the breadth of these complications [8], our understanding of the presentation, progression, and prevalence of most outcomes remains seriously incomplete [9]. Since CG is associated with extreme variability in chronic complications and/or long-term outcomes, even individuals who do not exhibit acute symptoms in the newborn period can develop language delay, speech defects, learning disabilities, cognitive impairment, and in females, POI [1].

CG has profound acute and long-term effects on the central nervous system potentially due to chronic intoxication with endogenously produced galactose and/or cell dysfunction due to metabolic derangement. In the setting of poor feeding, jaundice, and hepatomegaly, galactosemia has been shown to cause acute elevated intracranial pressure and diffuse cerebral edema [10]. Additionally, patients with CG frequently report difficulties in speech (60%) and most patients are also diagnosed with primary verbal dyspraxia or developmental apraxia of speech [11]. Despite early intervention, approximately 10-20% of galactosemia patients develop more severe ataxia and tremors [11].

In terms of the structural effects of CG on the brain, a small number of autopsy and imaging studies have revealed that GALT deficiency can lead to moderate cortical atrophy,

abnormal myelination, and hyperactivity in the periventricular white matter [12, 13]. These studies have also suggested that individuals with galactosemia can suffer from abnormalities in white matter development despite early diagnosis and treatment [13]. Another neuroimaging study with 21 patients with CG found a decrease in white matter volume, microstructure, and myelin both in the whole brain and corticospinal tract (CST). Galactosemic patients demonstrated both white matter and gray matter pathology, and more severe brain abnormalities on MRI correlated with poorer neurological and intellectual outcomes [14].

The Leloir Pathway of Galactose Metabolism

In most organisms, the conversion of β -D-galactose to metabolically favorable glucose 1-phosphate is achieved through the action of four enzymes that constitute the Leloir pathway (Figure 1). These include galactose mutarotase (GALM), galactokinase (GALK), galactose-1-phosphate uridylyltransferase (GALT), and UDP-galactose 4'-epimerase (GALE) [15]. In the first step of the pathway, β -D-galactose, liberated from lactose, is epimerized into α -D-galactose by GALM. Next, α -D-galactose is phosphorylated to form galactose-1-phosphate through ATP-dependent GALK. Subsequently, the GALT enzyme facilitates the conversion of galactose-1-phosphate and UDP-glucose to glucose-1-phosphate and UDP-galactose. Lastly, UDP-galactose is converted back to UDP-glucose by GALE.

Although the Leloir pathway is the main route of galactose metabolism in mammals, there are also alternate bypass pathways that convert galactose into other metabolites. For example, galactose can be oxidized to galactonate by galactose dehydrogenase, reduced to galactitol by aldose reductase, and converted to UDP-galactose by UDPglucose phosphorylase (UGP) [16]. While *GALT* is expressed in all tissues, the liver is the primary site of galactose

metabolism in mammals [17]. Patients with GALT deficiency exhibit persistent elevation of galactose metabolites in blood and other tissues, even on lactose-free diets. The biochemical basis for this elevation can be attributed to the endogenous production of galactose. ¹³C-labeled galactose studies have demonstrated the endogenous synthesis of galactose at the rate of 1mg/kg/hr in normal adults and patients with GALT deficiency [18]. The endogenous production of galactose (1.1-1.3g) per day exceeds the free galactose intake in adult galactosemic patients on lactose-restricted diets which could contribute to the pathogenesis of the long-term complications [19]. The level of endogenous galactose produced is even higher in children [20, 21].

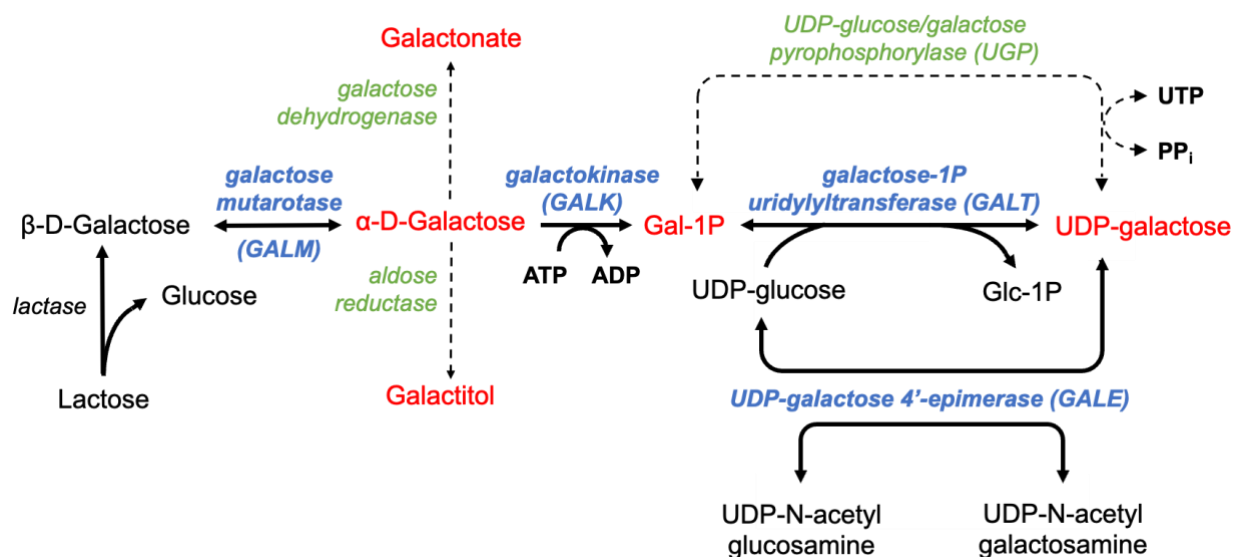


FIGURE 1: Leloir pathway of galactose metabolism. Galactose and galactose metabolites are presented in red. The primary enzymes of the pathway are represented in blue, and the alternate enzymes are illustrated in green (modified from Fridovich-Keil JL and Berry GT, 2022) [9].

Current Treatment and Gene-Based Therapeutic Approaches

The current therapeutic standard of care for galactosemic patients is a galactose-restricted diet which is effective in nullifying acute neonatal complications but is inadequate in preventing long-term complications. *GALT* gene therapy is currently being investigated as a potential

treatment to directly restore GALT activity. Based on the biochemical variant of galactosemia (Duarte Galactosemia), restoring GALT activity up to 25% is likely to rescue the phenotype of the clinical disease [22]. Gene therapy approaches treat genetic disorders by providing patients with the correct coding DNA (cDNA) sequence of the missing gene to produce the normal protein. The most important step in gene therapy is the efficient delivery of the transgene to the target cells/tissue, which is carried out by vehicles called vectors [23]. Conventionally, viral vector-based gene therapies are delivered *in vivo* by vectors such as adenoviruses (Ads), lentiviruses (LVs), and adeno-associated viruses (AAVs). In 2021, 50% of clinical trials employing viral vectors used Ads, while LVs and AAVs were used in 22% and 28% of clinical trials respectively [23]. Alternatively, the transgene can be delivered *ex vivo* which involves extracting cells from the patient and genetically modifying them outside of the body before reintroducing the cultured cells. Based on the study design, this review will only discuss AAV-mediated gene replacement *in vivo*.

In addition to the viral vector, the administration route is also important for targeted gene therapy *in vivo*. Numerous routes of administration that can be used to deliver a transgene into the brain are directly injecting into the parenchyma of the brain, injecting into cerebroventricular space, intrathecal (IT) administration into the cisterna magna or the lumbar area, intravenous injection, and intranasal administration [24]. In this study, lumbar IT administration was used to deliver the *GALT* transgene to the CNS. IT administration reduces the targeting of virus in peripheral organs and avoids AAV-neutralizing antibodies in the blood as compared to intravenous delivery [25]. Therefore, a lower dosage of the gene therapy can be injected into the subject which lowers the risk of an immune response.

The timing of gene therapy administration is also vital to the success of treatment. In AAV-mediated gene transfer studies for late infantile neuronal ceroid lipofuscinosis (Batten disease), the improvement of clinical outcomes was dependent on the age of the intervention [26, 27]. These studies reported that treatment at pre- or early-symptomatic ages resulted in considerably better outcomes compared with treatment after the emergence of symptoms and confirmed that earlier treatment maximizes the therapeutic effects.

Adeno-Associated Virus (AAV)-Mediated Therapy

AAV is widely used in research because it is non-pathogenic, non-replicating, low immunogenic, and predominantly non-integrating in humans [28]. It is essentially a protein shell protecting a single-stranded or double-stranded DNA genome of approximately 4.8 kilobases (kb) with a cargo packaging capacity of about 3.3 kb. Recombinant AAV (rAAV), which lacks viral DNA, is used to generate gene therapies and deliver the DNA into the nucleus of the cell [28]. The transgenes encoded within the rAAV can form circular concatemers that exist as episomes in the nucleus of the transduced cells [28]. Since rAAV lacks genes that are required for viral genome replication and predominantly does not integrate into the host genome, transgene expression is diluted over time as the cell undergoes mitosis. The rate of transgene loss is a function of the replication or turnover rate of the transduced cells.

The infection pathway is dependent on the serotype of the AAV; different serotypes bind to different cell surface glycoprotein receptors and secondary receptors or have differential affinities for these receptors. Clathrin-mediated endocytosis occurs upon binding to the cell surface. Infecting AAV particles are engulfed in endosomal vesicles and are transported through late endosomal compartments. The AAV capsid undergoes a conformational change that allows

the genome to escape. The genetic material is shuttled into the nucleus via a nuclear localization signal. If the genome is single-stranded, the second strand must be synthesized in the nucleus to form a double-stranded DNA required for transcription. Since this can act as a limiting step in transgene expression, self-complementary (double stranded) AAV (scAAV) can be utilized, if the payload is sufficiently small, so the viral genome can be transcribed immediately for faster transgene expression. One of the biggest advantages of rAAV as a gene vector is the lack of a viral genome and engineered lipids or other chemical components that could contribute to immunogenicity [28]. Although the AAV has demonstrated lower immunogenicity than other viruses, the capsid proteins and the nucleic acid sequence can trigger an immune response [23].

The choice of a particular AAV is dependent on the cell/tissue type being targeted and the desired method of delivery (systemic or local). Since AAV enters the cell through interactions with carbohydrates on the surface, subtle differences in the affinity for sialic acid, galactose, and heparin sulfate can influence cell-type transduction preferences [28]. For example, AAV9 preferentially binds to galactose and has the ability to cross the blood-brain barrier and infect the cells in the CNS [29]. Furthermore, secondary receptors such as hepatocyte growth factor receptor, epidermal growth factor receptor, and integrins are also critical for AAV cell binding and internalization [28]. As of now, 12 natural serotypes have been identified and studied as gene delivery vehicles with different tissue tropisms (Table 1) [30]. In this study, scAAV9 was used as the viral vector to deliver a *GALT* transgene to enable diverse tissue tropism and the ability to efficiently transduce neurons and glial cells.

TABLE 1. Properties of AAV serotypes (adopted from Li C and Jude Samulski, 2020) [30].

AAV serotype	Primary receptor	Co-receptor	Tissue tropism
AAV1	Sialic acid	AAVR	Muscle, CNS, heart
AAV2	Heparin	Integrin, FGFR, HGFR, LamR, AAVR	Liver, CNS, muscle
AAV3	Heparin	FGFR, HGFR, LamR, AAVR	Muscle, stem cells
AAV4	Sialic acid	Unknown	Eye, CNS
AAV5	Sialic acid	PDGFR, AAVR	CNS, lung, eye
AAV6	Heparin, sialic acid	EGFR, AAVR	Muscle, CNS, heart, lung
AAV7	Unknown	Unknown	Muscle, CNS
AAV8	Unknown	LamR, AAVR	Liver, muscle, pancreas, CNS
AAV9	Galactose	LamR, AAVR	Almost every tissue
AAV10	Unknown	Unknown	Muscle
AAV11	Unknown	Unknown	Unknown
AAV12	Unknown	Unknown	Nasal

AAVR, AAV receptor; EGFR, epidermal growth factor receptor; FGFR, fibroblast growth factor receptor; HGFR, hepatocyte growth factor receptor; LamR, laminin receptor 1; PDGFR, platelet-derived growth factor receptor.

The CG Rat Model

The Fridovich-Keil Lab created a GALT-null Sprague Dawley (SD) rat model for CG using the CRISPR-Cas9 gene editing technology through a collaboration with the Geurts Lab at the Medical College of Wisconsin. The M3 mutation was created with non-homologous end joining that introduced a 2-base pair insertion into exon 6 of the rat *Galt* locus. The *Galt*^{M3} mutation disrupts the his-pro-his active site of the GALT enzyme and produces a premature stop codon downstream. A single male with the *Galt*^{M3} mutation was confirmed using Sanger

sequencing and outbred to establish the SD-*Galt*^{M3} strain used in this study. The knock-out model was confirmed through GALT enzyme assays on samples of liver harvested from newborn wild-type (WT), *Galt*^{M3} heterozygous, and *Galt*^{M3} homozygous pups. The GALT activity detected in wild-type pups was twice as much as the heterozygotes and GALT activity was undetectable in *Galt*^{M3}/*Galt*^{M3} animals [31]. The mutation did not affect GALK and GALE activities.

The GALT-null rat model exhibits a range of phenotypes that are reminiscent of adverse outcomes seen in humans with CG including cataracts, mild-growth delay, cognitive impairment and motor deficits [31]. GALT-null pups display bilateral cataracts from the times their eyes first open (about P14); these cataracts remain visible into adulthood while WT and heterozygous rats (GALT+) do not display cataracts. In terms of growth delay, GALT-null rats weigh less than both heterozygous and WT pups at 1 day after birth and the size disparity persists at least through puberty[31]. The motor and cognitive deficits in GALT-null rats were quantified through a rotarod activity and Morris water maze with a hidden platform [31]. The M3 GALT-null rat also demonstrated metabolic consequences of GALT-deficiency through accumulation of galactose, galactitol and Gal-1P in all tissues in animals ranging from newborns to older adults [31].

His Pro His (GALT enzyme active site)

wild-type sequence: 5' ... TCT AAC CCC CAT CCC CAC TGC CAG GTT TGG GCT AGC AAT TTC CTG CCA GAT ATT GCC CAG CGT GAA GAG CGA ... 3'
rGALT^{M3} (2-bp insertion): 5' ... TCT AAC CCC CAC **CTC CCC ACT** GCC AGG TTT GGG CTA GCA ATT TCC TGC CAG ATA TTG CCC AGC GTG AAG AGC ... 3'

wild-type sequence: ... ser asn pro his pro his cys gln val trp ala ser asn phe leu pro asp ile ala gln arg glu glu arg ...
rGALT^{M3}: ... ser asn pro his leu pro thr ala arg phe gly leu ala ile ser cys gln ile leu pro ser val ... STOP

Figure 2. The *Galt*^{M3} mutation created by CRISPR-Cas9 gene editing in rat (adopted from Rasmussen SA, Daenzer JMI, et al., 2019) [31]

Neonatal AAV-mediated GALT Restoration Offers Metabolic and Phenotypic Partial Rescue

Previous studies in the lab have expressed human GALT (hGALT) in GALT-null rats using an adeno-associated viral vector (AAV9) administered intravenously in neonatal rats [32, 33]. GALT activity assays confirmed strong transgene expression in both liver and brain in all scAAV9-hGALT-treated rats harvested at day 8, with detectable GALT activity persisting through 60 days [33]. Immunohistochemistry and double-label immunofluorescence illustrated that GALT signal was present in at least frontal cortex, cerebellum, and hippocampus. Additionally, GALT staining was observed in neurons including Purkinje cells in the cerebellum. H&E-stained sections of liver and brain showed no visible pathology as a function of *GALT* genotype, *GALT* transgene expression level, or scAAV9 exposure. Furthermore, metabolic correction was achieved in liver, brain, and blood following GALT restoration in GALT-null rats. All three metabolites (galactose, galactitol, and GalIP), which were present at high levels in PBS-treated GALT-null rats, were lowered to normal levels at 8 and 14 days [33]. The metabolic correction persisted until 30 and 60 days, but it was not as complete as that observed in younger rats [33]. The level of GALT restoration achieved in both liver and brain was sufficient to minimize cataracts at day 30 and partially rescue the pre-pubertal growth delay [33].

Significance of the study

While gene therapy for CG may be most effective when administered at an early age, there are thousands of adolescent and adult galactosemic patients who may benefit from intervention to relieve their complications, even if partially. The quality of life of most of these patients is affected by the brain-related phenotypes such as cognitive, behavioral, motor and speech impairments. Hence, the overarching goal of the study described here is to test the

efficacy of scAAV9-mediated hGALT replacement administered intrathecally in adolescent rats. The current study had two goals. First, we wanted to determine if we can achieve GALT restoration in brain and possibly also other tissues following adolescent intrathecal administration of viral vector. Second, we wanted to evaluate the metabolic rescue in the brain and plasma of GALT-null rats following IT administration of scAAV9-hGALT. Beyond the scope of this study, we also plan to investigate whether intrathecal GALT restoration in adolescent rats modifies brain-related phenotypes.

In order to address these questions, we administered scAAV9.CBh.HA-hGALT to 28-30 day old M3/M3 rats by lumbar intrathecal injection. We injected WT/WT rats with PBS and M3/M3 rats with PBS as positive and negative controls respectively. We performed tissue collections at three timepoints: 1-month post injection, 2-months post injection, and 4-months post injection. The following table describes the cohort sizes for each comparison group at each timepoint (Table 2). To be clear, due to limitations with access to the high-performance liquid chromatography instrument (HPLC) needed to process these samples, we do not have data from all the samples described. The prioritized subset of samples is described in the results, and the remaining samples will be analyzed in the coming months.

TABLE 2. Cohort sizes of the treatment groups in the experiment.

Days after treatment	Genotype	Treatment	Count
30 days (1-month)	WT/WT	PBS	8
	M3/M3	PBS	8
	M3/M3	scAAV9.CBh.HA-hGALT	7
60 days (2-months)	WT/WT	PBS	5
	M3/M3	PBS	5
	M3/M3	scAAV9.CBh.HA-hGALT	5

120 days (4-months)	WT/WT	PBS	5
	M3/M3	PBS	5
	M3/M3	scAAV9.CBh.HA-hGALT	5

Chapter 2: GALT restoration in brain following adolescent intrathecal administration of scAAV9-hGALT

Introduction

Gene therapies are currently being investigated as a potential treatment for CG to directly restore GALT activity in various tissues. As this study aims to evaluate the effectiveness of the treatment in adolescents and young adults, it is crucial to assess the transgene expression in the brain. This is because brain-related phenotypes significantly impact the quality of life of these individuals, and quantifying the transgene transduction in the brain would provide valuable insights into the potential therapeutic benefits of the treatment for this specific population. Since AAV9 is a non-replicating and predominantly non-integrating vector, this section also focuses on the changes in transgene expression over the timeframe of the study to understand the kinetics of expression of IT administered hGALT in GALT-null rats. To address this goal, tissue collections were performed on WT/WT rats treated with PBS, M3/M3 rats treated with PBS, and M3/M3 rats treated with scAAV9.CBh.HA-hGALT 30 days, 60 days, and 120 days after treatment. The biochemical variant (Duarte) galactosemia has demonstrated that restoring GALT activity up to 25% rescues the adverse phenotypes and does not result in clinical disease [34]. Hence, the goal of this investigation was to achieve at least 25% GALT restoration in the brain and sustain it over the course of the study.

Materials and Methods

Rats and Rat Husbandry

Wild-type and GALT-null Sprague Dawley rats used in the study were maintained in space overseen by the Division of Animal Resources at Emory, and all procedures were

approved by the Emory Institutional Animal Care and Use Committee (IACUC) under protocol PROTO201700095 (PI: JL Fridovich-Keil). Pups were weaned at 24 days of age. All rats were weaned to ad libitum LabDiet 5053 chow, plus plain water (for a post-wean diet containing 1% of calories from galactose). Before weaning, all rats were nursed by their mothers; rat breast milk contains about 3% calories from galactose (Jenness et al 1974). All pups were weighed daily beginning the day after birth through 10 days post-injection. After that time, animals were weighed weekly until they were euthanized.

Viral Administration to Adolescent Rats

All intrathecal injections for this project were performed by Dr. Anthony Donsante at Emory University. Specifically, anesthesia was induced by placing the animals in a transparent box where 2% isoflurane was inhaled. 2% isoflurane exposure was maintained during the surgery using a nose cone. Buprenorphine was administered at the beginning of the surgery and lidocaine was administered to the wound just before closure. An incision was made overlying the L3 and S2 vertebrae. A 30-gauge insulin needle was inserted between L3 and L4 vertebra containing 33 μ L of vector or sterile 1X PBS to be injected (Figure 3) and carefully retracted after injection. The skin was stapled or sutured. Following surgery, the animal was held in the Trendelenburg position for up to 30 minutes, and then placed in a cage warmed on one side. The viral vector dosage used for this study was 5.4×10^{11} vg/rat.



FIGURE 3. Image of Dr. Anthony Donsante injecting 33 μ L of scAAV9.CBh.HA-hGALT into a GALT-null rat intrathecally. The animal is under anesthesia using 2% isoflurane inhaled through the nose cone during the surgery.

Euthanasia and Tissue Harvest

Rats were harvested 1-month, 2-months, and 4-months post injection after being euthanized under deep isoflurane anesthesia. Following anesthesia, the chest cavity was opened to expose the heart, and whole blood was withdrawn from the right atrium using a 27G needle into a 5-mL sodium heparin BD Vacutainer tube that was stored on ice until processing. Subsequently, a 23G needle was inserted into the left ventricle and perfusion with PBS was performed to remove blood from solid tissues. Solid tissues to be processed for enzyme assays or metabolite analyses were removed, cut with a razor, homogenized, flash frozen in liquid nitrogen, and stored in aliquots at -80°C until use. Tissues to be processed for histology were removed, submerged in 10% neutral-buffered formalin and incubated with gentle rocking for 72 hours prior to transfer to 70% ethanol and eventual paraffin embedding. The following tissues were collected: brain, spinal cord, liver, gonads, heart, eyes, spleen, lungs, and muscle.

The heparinized blood was transferred from the Vacutainer tube into two clear 1.5 microfuge tubes and centrifuged at 2000 revolutions per minute (RPM) for 15 minutes at 4 °C. Centrifugation separated plasma and RBCs based on their differential sedimentation rate. The top plasma layer was removed and aliquoted at 100 µL each into new tubes. Next, 1000 µL of 1X Phosphate Buffered Saline (PBS) was used to resuspend the RBC pellet. The tube was centrifuged again at 2000 RPM for 15 minutes. The top PBS layer was discarded, and the RBCs were aliquoted into new tubes. Like the solid tissues, aliquoted plasma and RBCs for each animal were stored in the -80°C until use.

GALT Enzyme Assays (adopted from Rasmussen SA, et al., 2021) [32]

Frozen soft tissues were thawed and ground on ice for approximately 30 seconds in 100 µL lysis buffer (one complete mini protease inhibitor cocktail pellet dissolved in 10 mL of 100mM glycine, pH 8.7) using a Teflon micro pestle and handheld micro pestle motor. For muscle, the TissueLyser LT was used to agitate a tube containing tissue, buffer and a 5 mm stainless steel bead at a frequency of 40 Hz for 2 minutes. Lysates were centrifuged at 16,110g to pellet solids and approximately 80 µL of the supernatant was passed through a Micro Bio-Spin P6 chromatography column to remove small molecules by centrifuging at 1000g for 4 minutes. Total protein concentration of each supernatant was determined using the Bio-Rad DC protein assay with bovine serum albumin as a standard. To ensure every enzyme assay was performed within the linear range, different protein amounts and lysate dilutions were used for the GALT assays for different tissues and genotypes (Table 3) [33]. These dilutions were determined empirically to yield GALT enzyme assays in the linear range for the enzyme.

TABLE 3. Amount of protein used for the GALT assays by genotype and tissue-type.

Genotype	Brain (μg)	Liver (μg)	Muscle (μg)
WT/WT	20	5	20
M3/M3	40	10	20

To initiate reactions, 30 μL of soluble lysate was added to 20 μL of premix containing reaction substrates, cofactors, and buffers [35]. Two replicates for the positive reaction were processed and one replicate of the negative reaction that did not contain gal1P was performed to identify the level of background conversion of UDP-glc to UDP-gal (by GALE). The gal-1P-plus premix contained 1 M glycylglycine, 100mM UDP glucose, gal1P, and sterile milli-q water. The gal-1P-minus premix lacked gal1P substrate thus preventing the conversion of UDP-glucose to UDP-galactose by GALT (but not by GALE). All reaction mixtures were incubated at 37°C for 30 minutes, followed by a quench with 450 μL of ice-cold HPLC-grade water. Reactions were passed through 0.22 μm Costar Spin0X centrifuge tube filters at 4000g for 4 minutes. The filter was removed from the tube and the samples were stored in a -80°C freezer until ready for HPLC separation and quantification.

GALT Quantifications

Reaction mixtures were removed from the freezer and allowed to thaw on ice. Since the GALT enzyme converts UDP glucose and gal1P into UDP galactose and glc1P, we wanted to quantify the amount of UDP galactose in the reaction mixture to calculate the enzyme activity. The reaction mixtures were filtered through the CarboPac PA10 analytical column that consisted of an amino trap column (4 x 50 mm) and borate trap column (4 x 50 mm) using 15 mM NaOH (Buffer A) and 50 mM NaOH/1 M NaAc (Buffer B) mobile phase buffers. The CarboPac PA10

column used a flow rate of 1 mL/min with the following ratios of each buffer: 85% Buffer A and 15% Buffer B for -5 to 5 minutes, linear increase in Buffer B to 70% for 1 to 27.5 minutes, hold of Buffer B at 70% for 27.5 to 37 minutes, then a linear decrease of Buffer B back to 15% for 37 to 44 minutes. The injection volume for all samples was 20 μ L, and the autosampler was chilled prior to loading of the samples.

The GALT standards run to create the standard curve for the PA10 column were 1x, 5x, and 10x dilutions. A 10 mL 10x stock solution of the GALT standard consisted of 100 μ L of 10 nmol/ μ L of gal1P, 100 μ L of 10nmol/ μ L of glc1P, 150 μ L of 20 nmol/ μ L, 300 μ L of 10 nmol/ μ L UDPglc, and 9350 μ L of HPLC-grade water. With each run, the HPLC generated a chromatogram depicting the elution times of each component of the sample. The peaks for the UDPgal and UDPglc were identified based on the elution time of the standards as well as the location of the peaks of interest relative to other identifiable peaks. For both UDPgal and UDPglc, the peaks were integrated through the Chromeleon software that automatically calculated the area under the peak. The Chromeleon software then calculated the pmol of the two compounds in the sample based on the integrated peaks and the standard curve for each compound.

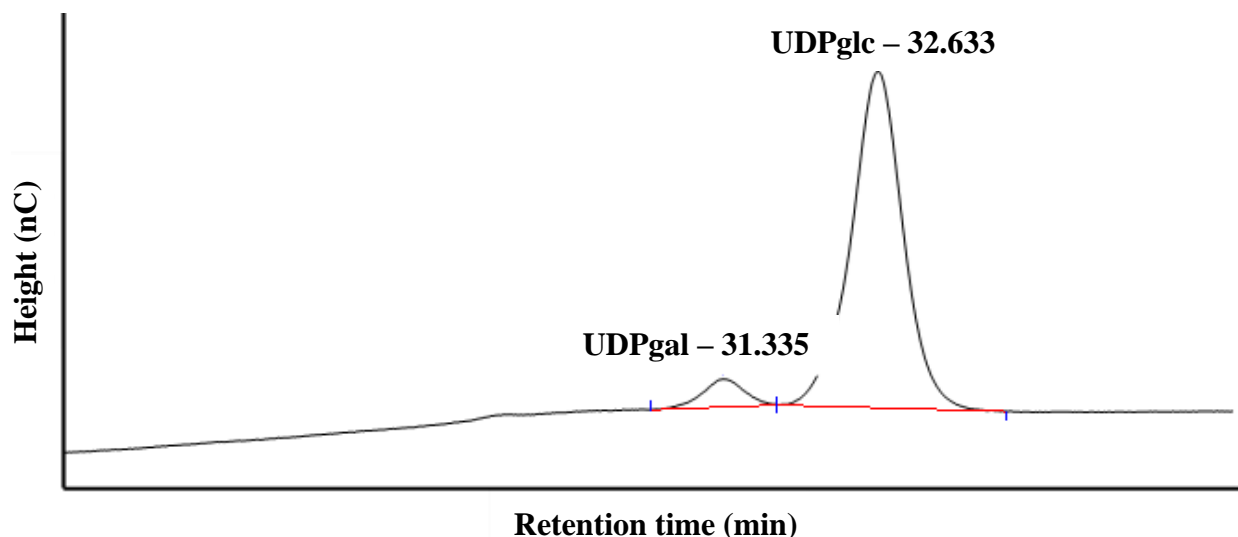


Figure 4. Chromatogram of a brain sample processed on the PA10 column with UDP galactose and UDP glucose peaks integrated in red. Each metabolite is labeled with their retention time in minutes.

The negative reaction was used to calculate the blanked UDPgal to account for the background in the reaction mixture; this background was subtracted from each Gal-1P containing reaction prior to calculating the level of GALT activity present.

$$\text{blanked pmol UDPgal} = \text{average pmol UDPgal (positive rxn)} - \text{pmol UDPgal (negative rxn)}$$

After the blanked pmol of UDPgal was calculated, the pmol UDPgal per reaction was calculated.

$$\text{pmol UDPgal per rxn} = \frac{(\text{blanked pmol UDPgal})}{(\text{injection volume} = 20 \mu\text{L})} \times (\text{rxn mixture total volume} = 500 \mu\text{L})$$

Lastly, the amount of UDPgal per reaction was standardized for the amount of protein used for the reaction. The enzyme activity was reported as pmol of product (UDP-gal) formed per μg of total protein per minute of reaction time.

$$pmol\ UDPgal\ per\ \mu g\ protein\ per\ min = \frac{\frac{pmol\ UDPgal\ per\ rxn}{\mu g\ protein}}{30\ min\ rxn\ time}$$

Sample Size

Due to time constraints and the reality of sharing an HPLC between multiple projects, GALT quantitation data has only been collected for a subset of the total samples. The following tables describe the samples analyzed for each brain and liver so far.

TABLE 4. Brain samples analyzed for Chapter 2

Time post injection	Genotype	Treatment	n
30 days (1-month)	WT/WT	PBS	8
	M3/M3	PBS	7
	M3/M3	scAAV9.CBh.HA-hGALT	7
60 days (2-months)	WT/WT	PBS	4
	M3/M3	PBS	3
	M3/M3	scAAV9.CBh.HA-hGALT	5
120 days (4-months)	WT/WT	PBS	3
	M3/M3	PBS	4
	M3/M3	scAAV9.CBh.HA-hGALT	5

TABLE 5. Liver samples analyzed for Chapter 2

Time post injection	Genotype	Treatment	n
30 days (1-month)	WT/WT	PBS	6
	M3/M3	PBS	5
	M3/M3	scAAV9.CBh.HA-hGALT	7
60 days (2-months)	WT/WT	PBS	1
	M3/M3	PBS	2
	M3/M3	scAAV9.CBh.HA-hGALT	3

120 days (4-months)	WT/WT	PBS	1
	M3/M3	PBS	2
	M3/M3	scAAV9.CBh.HA-hGALT	3

Statistical Methods

The degree of GALT restoration achieved in GALT-null rats was assessed by comparing the brain and liver GALT activities between M3/M3 PBS-treated rats and M3/M3 scAAV9.CBh.HA-hGALT-treated rats. All graphing and statistical calculations were performed in R Studio. The Wilcoxon Test was used to determine the overall significance at $\alpha = 0.05$ for graphs that compared enzyme activity at a specific time-point. Furthermore, the brain GALT activity over time for each experimental group was analyzed using the Kruskal-Wallis Test due to non-parametric data. Subsequently, pairwise Wilcoxon Tests were performed to compare the significance between various time-points. The Benjamini and Hochberg correction was applied to account for multiple tests and control for the false discovery rate [36].

Results

GALT activity assays confirmed transgene expression in the brain of all treated rats harvested 30 days after treatment (Figure 5), with detectable GALT activity persisting throughout the timeframe of the study (Figure 6-7). Although the transgene expression achieved GALT restoration that was approximately 15% of WT level, the enzyme activity did not diminish significantly over four months (Figure 10). In comparison, the GALT activity of M3/M3 rats treated with PBS remained around zero (Figure 9), while WT/WT rats displayed substantially higher activity that remained relatively constant throughout the study (Figure 8). Moreover, liver and muscle GALT assays were performed to detect any systemic leakage of the

virus from the spinal column to the bloodstream and body. No detectable GALT activity was found in the liver or muscle 30 days after treatment (Figure 12,15). As expected, the GALT activity in the liver remained undetectable 60 and 120 days after treatment (Figure 13,14).

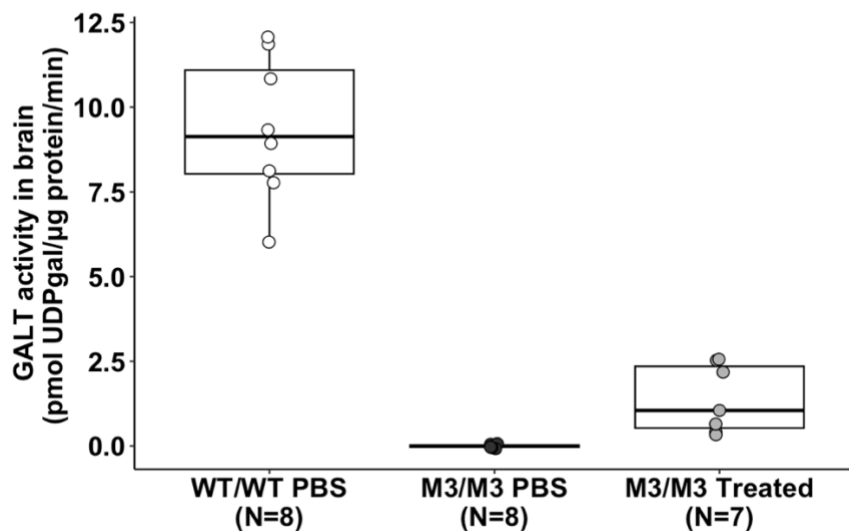


FIGURE 5. GALT activity in brains of PBS-treated WT rats (white symbols), PBS-treated GALT-null rats (black symbols), and scAAV9-hGALT-treated GALT-null rats (gray symbols) **one month after treatment**. Pairwise comparison between M3 PBS and M3 treated group ($P < 0.001$, Wilcoxon Test).

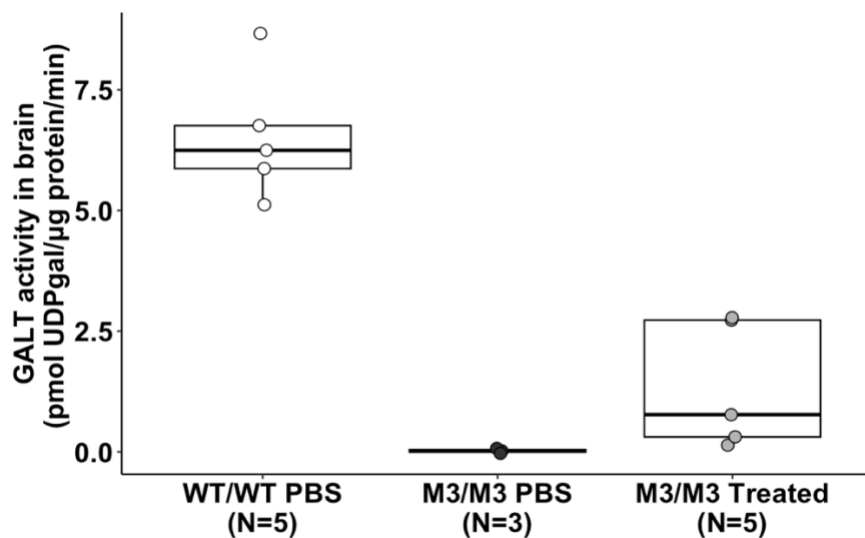


FIGURE 6. GALT activity in brains of PBS-treated WT rats (white symbols), PBS-treated GALT-null rats (black symbols), and scAAV9-hGALT-treated GALT-null rats (gray symbols)

two months after treatment. Pairwise comparison between M3 PBS and M3 treated group ($P = 0.0357$, Wilcoxon Test)

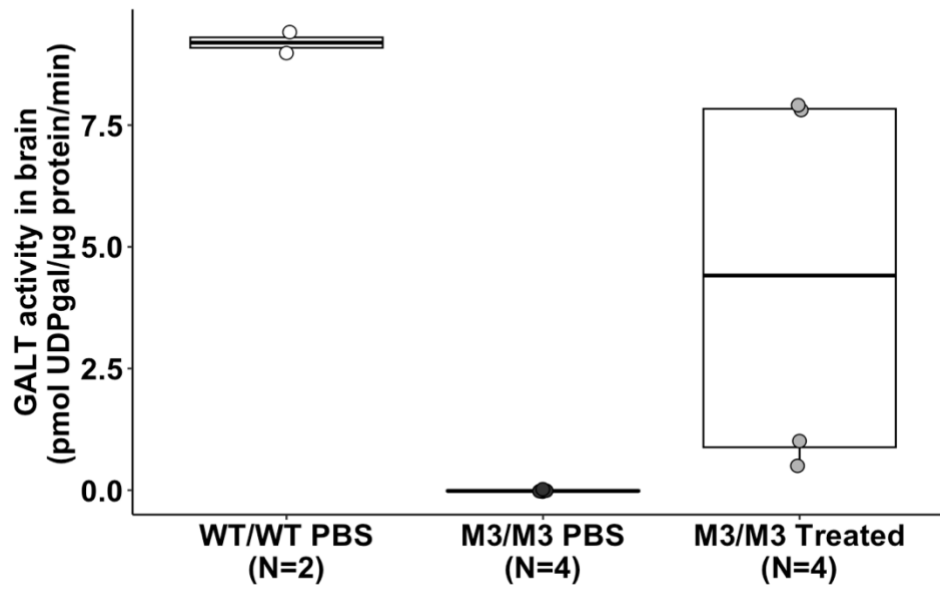


FIGURE 7. GALT activity in brains of PBS-treated WT rats (white symbols), PBS-treated GALT-null rats (black symbols), and scAAV9-hGALT-treated GALT-null rats (gray symbols) **four months after treatment.** Pairwise comparison between M3 PBS and M3 treated group ($P = 0.0357$, Wilcoxon Test)

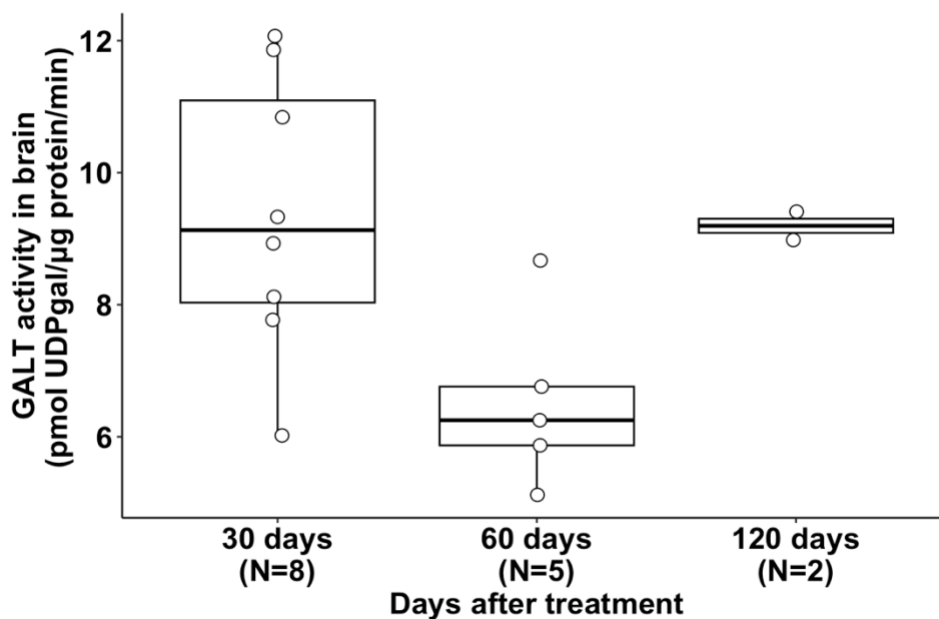


FIGURE 8. GALT activity over time in brains of WT rats treated with PBS. Pairwise comparisons performed between 30 and 60 days ($P = 0.089$, Wilcoxon Test), and 60 and 120 days ($P = 0.143$, Wilcoxon Test).

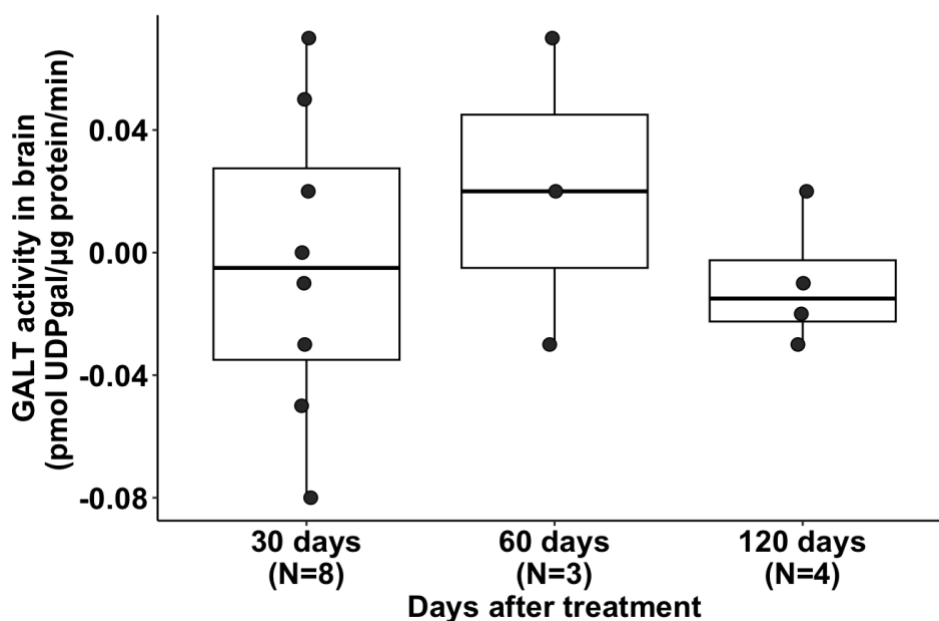


FIGURE 9. GALT activity over time in brains of M3/M3 rats treated with PBS. Pairwise comparisons performed between 30 and 60 days ($P = 0.860$, Wilcoxon Test), and 60 and 120 days ($P = 0.860$, Wilcoxon Test).

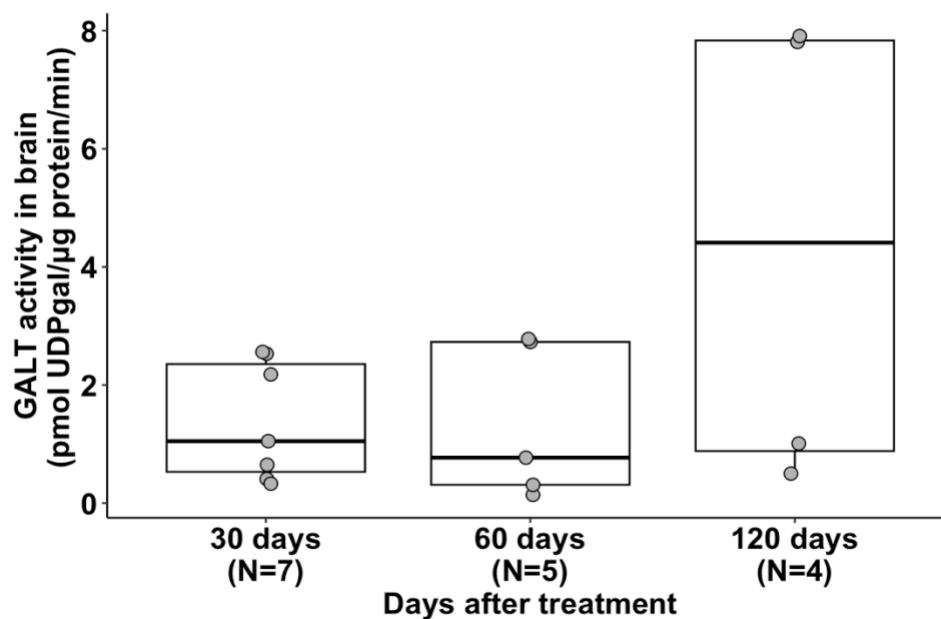


FIGURE 10. GALT activity over time in brains of M3/M3 rats treated with scAAV9.CBh.HA-hGALT. Pairwise comparisons performed between 30 and 60 days ($P = 1.00$, Wilcoxon Test), and 60 and 120 days ($P = 0.62$, Wilcoxon Test).

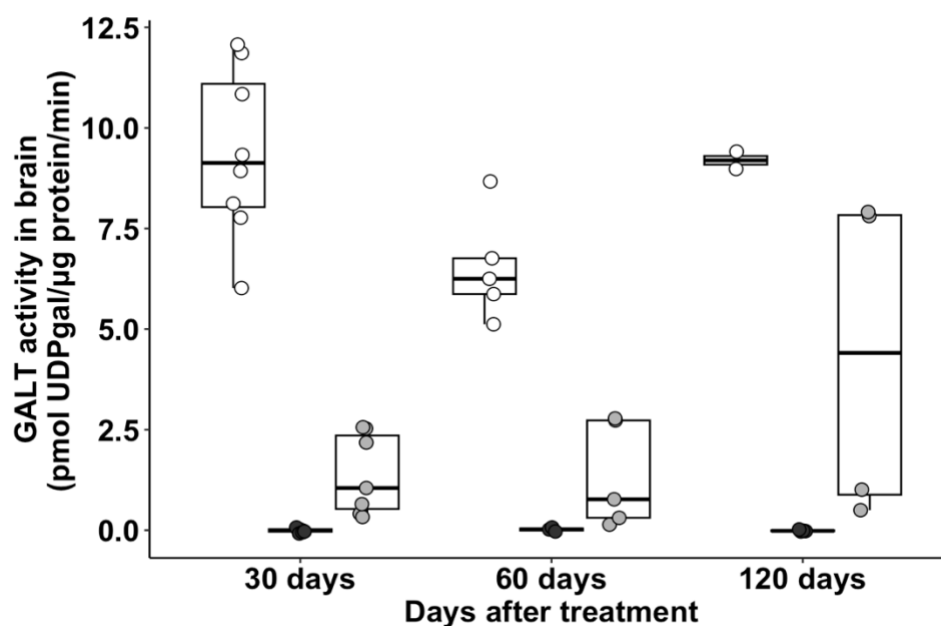


FIGURE 11. GALT activity over time in brains of PBS-treated WT rats (white symbols), PBS-treated GALT-null rats (black symbols), and scAAV9-hGALT-treated GALT-null rats (gray symbols).

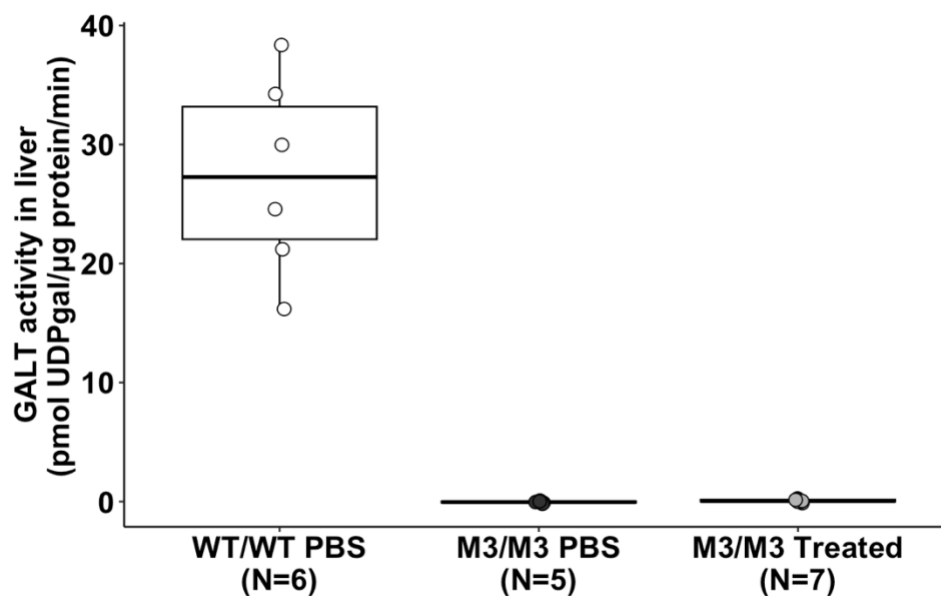


FIGURE 12. GALT activity in livers of PBS-treated WT rats (white symbols), PBS-treated GALT-null rats (black symbols), and scAAV9-hGALT-treated GALT-null rats (gray symbols) **one month after treatment**. Pairwise comparison between M3 PBS and M3 treated group ($P = 0.2020$, Wilcoxon Test).

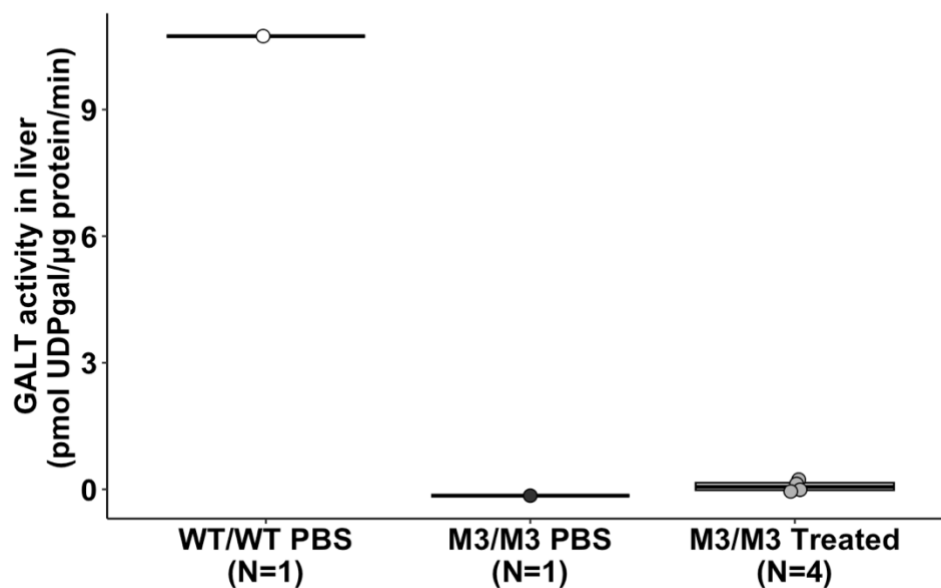


FIGURE 13. GALT activity in livers of PBS-treated WT rats (white symbols), PBS-treated GALT-null rats (black symbols), and scAAV9-hGALT-treated GALT-null rats (gray symbols) **two months after treatment**.

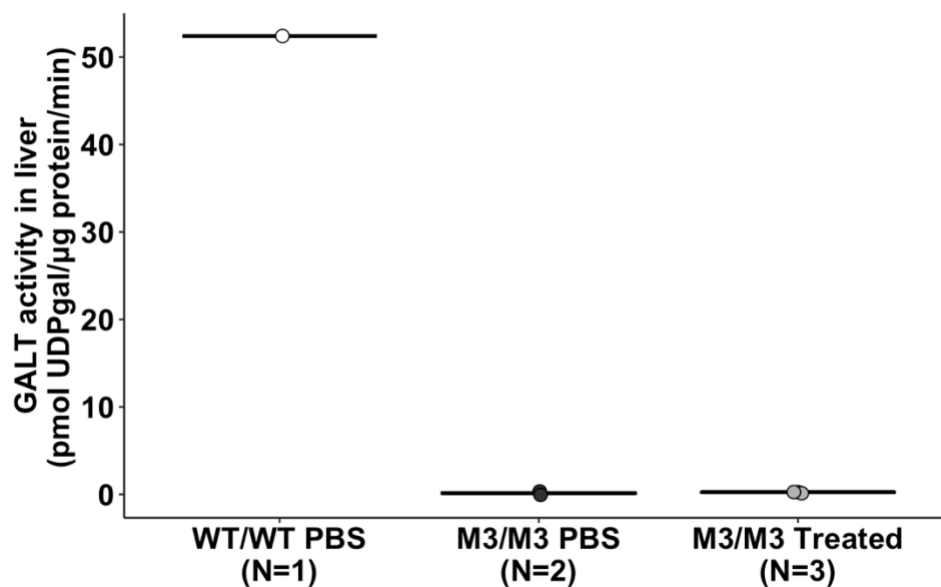


FIGURE 14. GALT activity in livers of PBS-treated WT rats (white symbols), PBS-treated GALT-null rats (black symbols), and scAAV9-hGALT-treated GALT-null rats (gray symbols) **four months after treatment.**

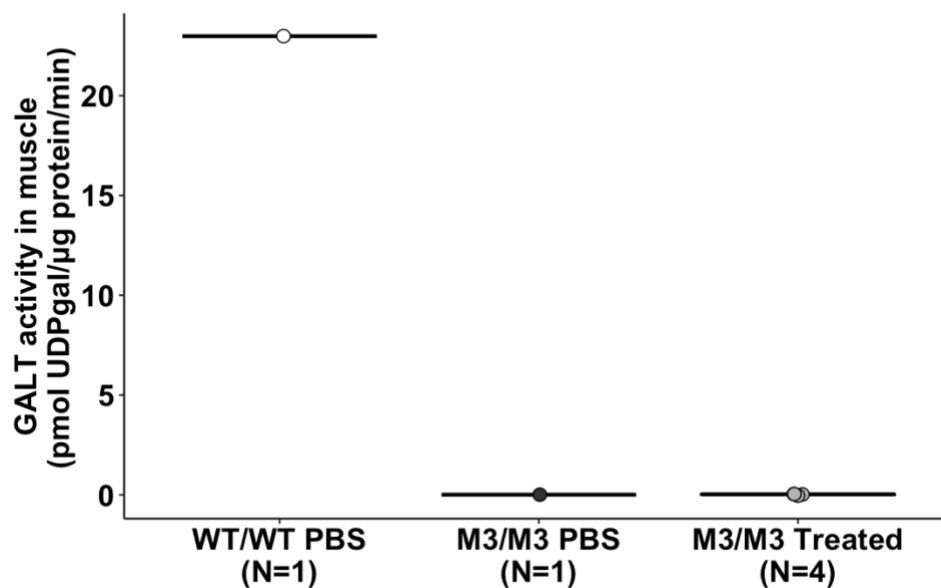


FIGURE 15. GALT activity in muscles of PBS-treated WT rats (white symbols), PBS-treated GALT-null rats (black symbols), and scAAV9-hGALT-treated GALT-null rats (gray symbols) **one month after treatment.**

Discussion

The enzyme activity data demonstrated notable transgene expression in the brains of treated GALT-null rats at all time points tested in the study (Figures 5-7). Interestingly, brain GALT activity remained relatively constant over four months for all three experimental groups (Figures 8-10). Previously, IV administration of scAAV9.CBh.HA-hGALT in neonatal rats (day 2 of life) showed strong transgene expression at day 8, and the brain GALT activity diminished significantly over 60 days in rats treated with hGALT. This drop in expression could be explained by the high growth rate in young rats compared to the adolescent rats in the study. Albeit IT administration of the treatment in this study was able to sustain the brain GALT enzyme activity level four months after treatment.

Although the rats treated with hGALT had discernable activity, it was only approximately 15% of the WT level. These results did not address whether the treatment had leaked into other tissues to reduce the overall transduction in the brain. Previous MRI studies have shown that acute lumbar injection often results in primarily spinal cord transduction due to the natural flow of CSF in the spine [37]. CSF descends along the dorsal region of the spine and spinal canal and ascends through the ventral side to the base of the brain. Hence, the liver was investigated to detect any systemic leakage of the treatment and no GALT activity was detected (Figures 12-14). To be clear, this does not necessarily mean that virus did not transduce hepatocytes at all because minute amounts of activity could have been present right after treatment and the activity could have been below the threshold of detection by the time of euthanasia.

To further investigate the transduction possibility in other tissues, we analyzed muscle because virus DNA delivered to the muscle usually leads to more persistent expression without

significant loss over time [38]. However, GALT activity was also undetectable in the muscle (Figure 15), which suggests that no significant leakage occurred in the investigated tissues. However, we analyzed a set of 4 spinal cords from treated rats, and we observed substantial activity in two of the rats. This suggests that the treatment could have been sequestered in the spinal columns of some animals resulting in low brain transgene expression. These data confirmed that we can successfully transduce hGALT in the brain using IT injection and that the restored GALT activity persists for at least four months with fairly high tissue specificity. These results could be the basis to study brain-related phenotypes in these rats to test the cognitive and behavioral effects of *GALT* transgene expression in GALT-null rats.

Chapter 3: Metabolic efficacy in brain and plasma of GALT-null rats following adolescent intrathecal administration of scAAV9-hGALT

Introduction

Previous studies have suggested that the profound acute and long-term phenotypes of CG may be a result of chronic intoxication with endogenously produced galactose and/or cell dysfunction due to accumulation of galactose-derivative metabolites in different tissues [1, 6, 10, 12]. The aim of this investigation was to characterize the changes in metabolite levels in GALT-null rats following IT administration of scAAV9.CBh.HA-hGALT. We wanted to examine whether GALT restoration in the brain could rescue metabolic intoxication in the brain and/or elsewhere in the body – represented by the plasma. To address this goal, we performed tissue collections on WT/WT rats treated at day 28-30 with PBS, M3/M3 rats treated with PBS, and M3/M3 rats treated with scAAV9.CBh.HA-hGALT at 30 days, 60 days, and 120 days after IT injection. Prior studies have showed a steady drop in galactose metabolite levels in untreated or PBS-treated GALT-null rats potentially due to a combination of increased UGP activity that converts Gal1P to UDP galactose [33], or decreased endogenous production of galactose [39]. Hence, the goal of this study was to quantify the extent and kinetics of metabolic rescue in brain and plasma of scAAV9.CBh.HA-hGALT-treated GALT-null rats relative to PBS-treated controls.

Materials and Methods

Wild-type and GALT-null Sprague Dawley rats used in the study were maintained in space overseen by the Division of Animal Resources at Emory, and all procedures were approved by the Emory Institutional Animal Care and Use Committee (IACUC) under protocol

PROTO201700095 (PI: JL Fridovich-Keil). The same rats used to analyze GALT activity (Chapter 2) were also used to measure the metabolite levels in tissues, and therefore, they were maintained, treated, and euthanized as described in the methods section of Chapter 2.

Metabolic Extractions

Brain and plasma metabolites were measured as described previously [31]. For brains, 100-110 mg of tissue were aliquoted into a 1.5 mL microfuge tube. For plasma, 100 μ L of fluid were aliquoted into a 1.5 mL microfuge tube. The metabolite extraction procedure was identical for both tissues. Frozen soft tissues were thawed and ground on ice for approximately 30 seconds in 125 μ L of ice-cold HPLC-grade water using a Teflon micro pestle and handheld micro pestle motor. 250 μ L of HPLC-grade 100% methanol (MeOH) and 500 μ L of HPLC-grade chloroform (CHCl_3), both chilled to -20 $^{\circ}\text{C}$, were added to each tube to separate both polar and non-polar metabolites from other cellular substances [40]. Subsequently, the samples were agitated on a vortex mixer at maximum speed for 45 minutes and centrifuged at 2000 RPM for 20 minutes at 4 $^{\circ}\text{C}$. The top aqueous layer was removed into a new 1.5 mL microfuge tube and placed on ice. 250 μ L of a 1:1 mixture of HPLC-grade water and HPLC-grade 100% MeOH, both chilled to -20 $^{\circ}\text{C}$, were added to each remaining bottom CHCl_3 layer. The bottom layer was re-extracted by vortex agitation of these tubes for 5 minutes followed by centrifugation at 2000 RPM for 20 minutes at 4 $^{\circ}\text{C}$. After the re-extraction, the top aqueous layer from the original tube was removed and combined with the top layer in the second tube on ice. The remaining tube containing the bottom CHCl_3 layer, and the solid tissue, was disposed in the designated CHCl_3 chemical waste container. The top aqueous layer tube was dried in the SpeedVac with no heat, for about 2-4 hours until no more fluid was visible. Dried metabolite pellets were resuspended in

200 μ L of ice-cold HPLC-grade water. The resuspensions were passed through 0.22 μ m Costar SpinOX centrifuge tube filters at 4000g for 4 minutes. The filter was removed from the tube and samples were stored in a -80 °C freezer until ready for HPLC analysis [31].

Metabolite Quantifications

Metabolites were removed from the freezer and allowed to thaw on ice. All metabolites were diluted with HPLC-grade water for optimal interpretation of the HPLC results based on standard curves, as presented in the following tables (Tables 6-7). All dilutions are listed as parts metabolite to parts HPLC-grade water. A dilution of 1:0 for plasma metabolites indicates that the samples were analyzed undiluted on the HPLC.

TABLE 6. Dilutions used for brain metabolites by genotype and time post-treatment of rats.

Genotype	1-month post injection	2-months post injection	4-months post-injection
WT/WT	1:3	1:2	1:2
M3/M3	1:3	1:2	1:2

TABLE 7. Dilutions used for plasma metabolites by genotype and time post-treatment of rats.

Genotype	1-month post injection	2-months post injection	4-months post-injection
WT/WT	1:0	1:0	1:0
M3/M3	1:0	1:0	1:0

Galactose and galactitol were filtered through an amino trap column (4 x 50 mm) and borate trap column (4 x 50 mm) using 1 M NaOH (Buffer A) and 15 mM NaOH (Buffer B) on a CarboPac MA1 analytical column (4 x 250 mm). The CarboPac MA1 column used a flow rate of 0.4 mL/min with the following ratios of the 2 buffers: 30% Buffer A and 70% Buffer B for -5 to

43 minutes, 70% Buffer A and 30% Buffer B for 43 to 45 minutes using linear increases and decreases from the starting ratio, then hold at 70% Buffer A and 30% Buffer B from 45 to 50 minutes[31]. Gal-1P was separated using the CarboPac PA10 analytical column (250 x 4 mm), with an amino-trap column (50 x 14 mm) placed in front of the analysis column and a borate-trap column (50 x 4 mm) placed in front of the injector port. 15 mM NaOH (Buffer A) and 50 mM NaOH/1M NaAC (Buffer B) mobile phase buffers were used. A 50% sodium hydroxide solution was added while preparing the buffers to prevent carbonate contamination of the analysis column[41]. The CarboPac PA10 column used a flow rate of 0.8 mL/min with the following ratios of each buffer: 90% Buffer A and 10% Buffer B for -5 to 1 minutes, linear increase of Buffer B to 65% from 1 to 30 minutes, hold of Buffer B at 65% from 30 to 52 minutes, then a linear decrease of Buffer B back to 10% from 52 to 54 minutes. The injection volume for all samples on both columns was 20 μ L, and the autosampler tray was chilled prior to loading of the samples.

The brain metabolite samples were run on both MA1 and PA10 columns to quantify the concentration of galactose, galactitol, and Gal-1P. The plasma samples were only run on the MA1 column because Gal-1P is an intracellular metabolite that is absent from the plasma [42]. A 1000 μ L 10x stock solution of the MA1 standard consisted of 50 μ L of 10 nmol/ μ L myo-inositol, 100 μ L of 10 nmol/ μ L galactitol, 50 μ L of 10 nmol/ μ L glucose, 50 μ L of 10 nmol/ μ L galactose, and 9750 μ L of HPLC-grade water. Additionally, a 1000 μ L 10x stock solution of the PA10 standard consisted of 50 μ L of 10 nmol/ μ L 2D galactose, 50 μ L of 10 nmol/ μ L glucose, 400 μ L of 10 nmol/ μ L Gal-1P, 100 μ L of 10 nmol/ μ L Glc1P, 100 μ L of 10 nmol/ μ L fructose-1-phosphate (Fruc-1P), 50 μ L of 10 nmol/ μ L fructose-6-phosphate (Fruc-6P), 100 μ L of 10 nmol/ μ L glucose-6-phosphate (Glc-6P), 100 μ L of 10 nmol/ μ L galactonate, 50 μ L of 10

nmol/ μ L UDP-gal, 100 μ L of 10 nmol/ μ L UDP-glc, 5 μ L of 20 nmol/ μ L UDP N-acetylgalactosamine (UDPgalNac), 10 μ L of 10 nmol/ μ L UDP N-acetylglucosamine (UDPglcNac), and 8885 μ L of HPLC-grade water.

The HPLC run generated a chromatogram for each sample depicting the elution times for each metabolite in the solution. The peaks for the relevant metabolites were identified based on the elution time of the standard and the location of the peaks relative to other identifiable peaks in the sample. The galactose and galactitol peaks on the MA1 column, and Gal1P peaks on the PA10 column, were integrated using Chromeleon software that calculated the area under the peaks. Based on the standard curve for each metabolite produced from the known concentrations, the Chromeleon software calculated the pmol of that metabolite in each sample based on the integrated peak areas.

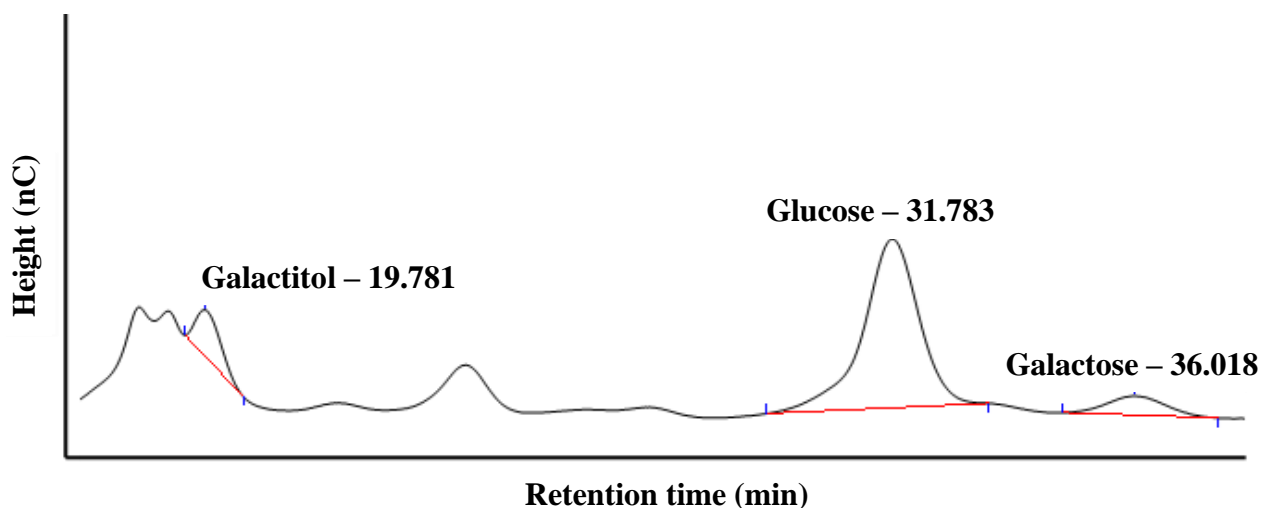


FIGURE 16. Chromatogram of a brain sample processed on the MA1 column with galactitol, glucose, and peaks integrated in red. Each metabolite is labeled with retention time.

The pmol of each metabolite in brain and plasma samples from rats collected at different ages were standardized using the following equation that accounted for the dilution factor and the initial mass (or volume) of the tissue processed:

For brain metabolites

pmol of metabolite per mg tissue

$$= \frac{(\text{pmol of metabolite in sample})(\text{dilution factor})(\text{resuspension volume} = 200 \mu\text{L})}{(\text{injection volume} = 20 \mu\text{L})(\text{mg tissue})}$$

For plasma metabolites

pmol of metabolite per μL plasma

$$= \frac{(\text{pmol of metabolite in sample})(\text{resuspension volume} = 200 \mu\text{L})}{(\text{injection volume} = 20 \mu\text{L})(100 \mu\text{L plasma})}$$

Sample size

Due to time constraints and limited availability of HPLC access due to other concurrent projects in the lab, metabolite quantification data has only been collected from a subset of the total samples. The following tables describe the samples currently analyzed for each tissue at the three time points. Since plasma samples do not require euthanasia, we were able to increase the sample numbers for the 1-month post injection group by analyzing the tail vein blood samples drawn from the animals that were euthanized at later timepoints.

TABLE 8. Brain samples analyzed in Chapter 3

Time post injection	Genotype	Treatment	n
1-month	WT/WT	PBS	8
	M3/M3	PBS	7
	M3/M3	scAAV9.CBh.HA-hGALT	7
2-months	WT/WT	PBS	5
	M3/M3	PBS	3
	M3/M3	scAAV9.CBh.HA-hGALT	5
4-months	WT/WT	PBS	3
	M3/M3	PBS	4
	M3/M3	scAAV9.CBh.HA-hGALT	5

TABLE 9. Plasma samples analyzed in Chapter 3

Time post injection	Genotype	Treatment	n
Prior injection	WT/WT	PBS	5
	M3/M3	PBS	5
	M3/M3	scAAV9.CBh.HA-hGALT	6
1-month	WT/WT	PBS	7
	M3/M3	PBS	9
	M3/M3	scAAV9.CBh.HA-hGALT	12
2-months	WT/WT	PBS	4
	M3/M3	PBS	3
	M3/M3	scAAV9.CBh.HA-hGALT	5
4-months	WT/WT	PBS	3
	M3/M3	PBS	4
	M3/M3	scAAV9.CBh.HA-hGALT	5

Statistical Methods

The metabolic efficacy of the treatment in GALT-null rats was assessed by comparing brain and plasma metabolites (galactitol, galactose and gal1P for brain and galactitol and galactose for plasma) between M3/M3 PBS-treated rats and M3/M3 scAAV9.CBh.HA-hGALT-treated rats. All graphing and statistical calculations were performed in R Studio. The Wilcoxon Test was used to determine the overall significance at $\alpha = 0.05$ for comparisons of the amount of metabolite at a specific time-point. The metabolite levels over time for each experimental group were analyzed using the Kruskal-Wallis Test due to non-parametric data. Subsequently, pairwise Wilcoxon Tests were performed to compare the significance between various time-points. The Benjamini and Hochberg correction was applied to account for multiple tests and control for the false discovery rate [36].

Results

Extent and Kinetics of Metabolic Rescue in Brain

Galactitol levels in the brains of M3/M3 rats treated with scAAV9.CBh.HA-hGALT showed a significant decrease 30 days after treatment compared to M3/M3 rats treated with PBS (Figures 17, 20, 23). At 60 days and 120 days after treatment, although the galactitol levels of M3/M3 rats treated with scAAV9.CBh.HA-hGALT were still trending lower than their PBS-treated counterparts, the difference was no longer statistically significant. Similarly, galactose levels in the brains of M3/M3 virus-treated rats did not show a significant difference from PBS-treated rats at any time points tested (30 days, 60 days, or 120 days) after treatment (Figure 18, 21, 24). Likewise, Gal1P levels were mostly unaffected by treatment at all timepoints tested (Figures 19, 22, 25), potentially because Gal1P is a strictly intracellular metabolite so that the GALT in a small number of transduced cells is not able to lower Gal1P levels in their non-transduced neighboring cells. Over time, galactitol levels remained relatively constant for both WT/WT rats treated with PBS and M3/M3 rats treated with PBS (Figures 26, 27). Interestingly, galactitol levels increased over time for M3/M3 rats treated with scAAV9.CBh.HA-hGALT (Figure 28). On the contrary, galactose and Gal1P levels did not change significantly over time for any of the experimental groups (Figures 29-34). Whether these differences are meaningful or reflect statistics of small numbers is difficult to determine from this pilot study.

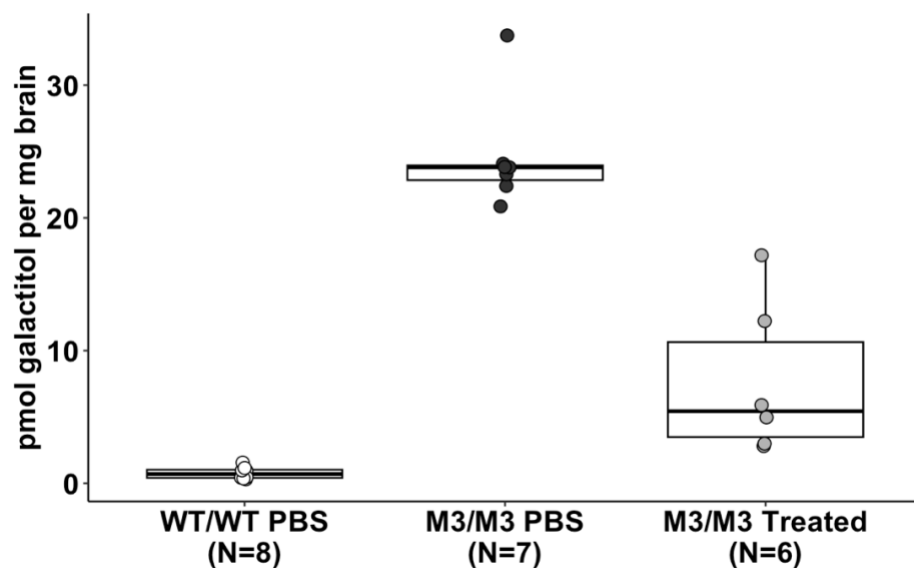


FIGURE 17. Galactitol levels in brains of PBS-treated WT rats (white symbols), PBS-treated GALT-null rats (black symbols), and scAAV9-hGALT-treated GALT-null rats (gray symbols) **one month after treatment**. Pairwise comparison between M3 PBS and M3 treated group ($P = 0.0012$, Wilcoxon Test).

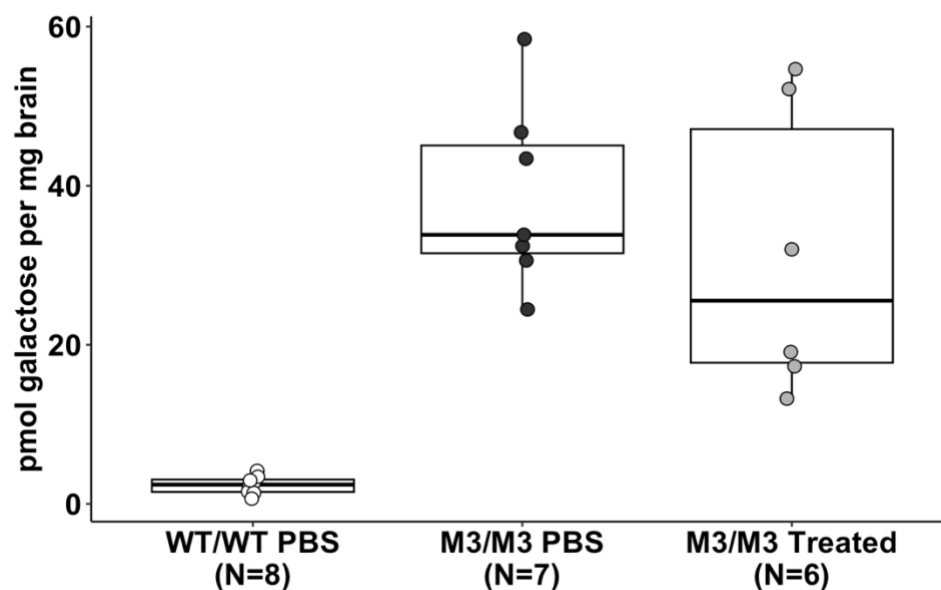


FIGURE 18. Galactose levels in brains of PBS-treated WT rats (white symbols), PBS-treated GALT-null rats (black symbols), and scAAV9-hGALT-treated GALT-null rats (gray symbols) **one month after treatment**. Pairwise comparison between M3 PBS and M3 treated group ($P = 0.3660$, Wilcoxon Test).

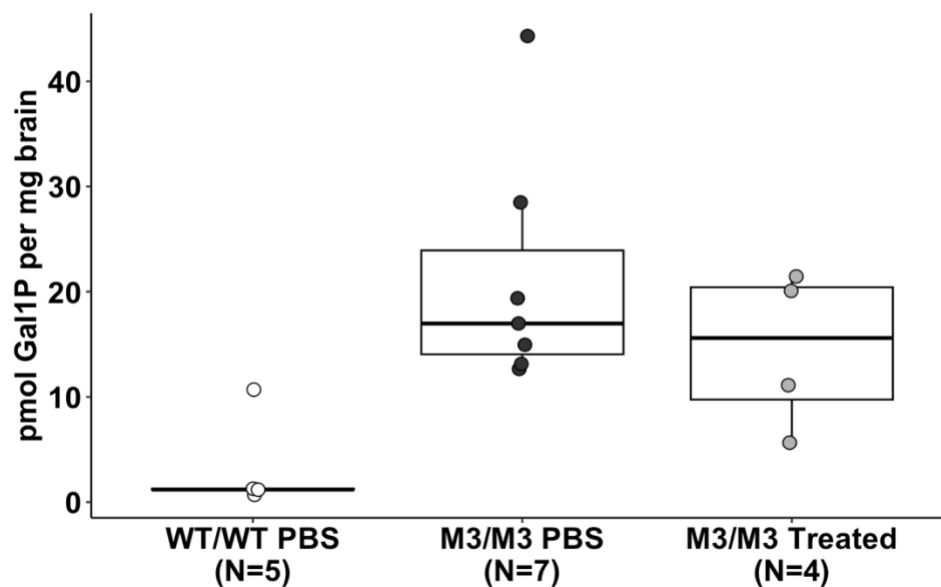


FIGURE 19. Gal1P levels in brains of PBS-treated WT rats (white symbols), PBS-treated GALT-null rats (black symbols), and scAAV9-hGALT-treated GALT-null rats (gray symbols) **one month after treatment**. Pairwise comparison between M3 PBS and M3 treated group ($P = 0.5273$, Wilcoxon Test).

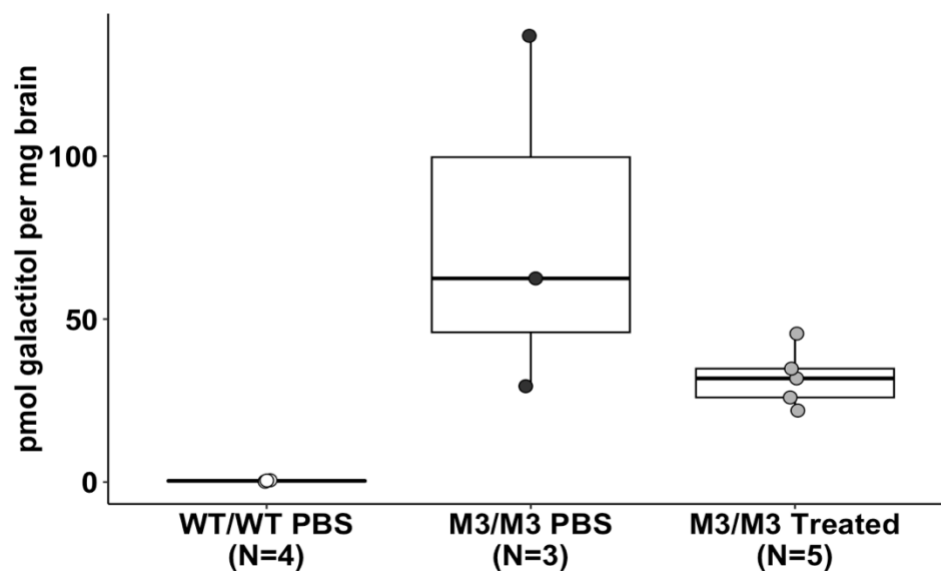


FIGURE 20. Galactitol levels in brains of PBS-treated WT rats (white symbols), PBS-treated GALT-null rats (black symbols), and scAAV9-hGALT-treated GALT-null rats (gray symbols) **two months after treatment**. Pairwise comparison between M3 PBS and M3 treated group ($P = 0.250$, Wilcoxon Test).

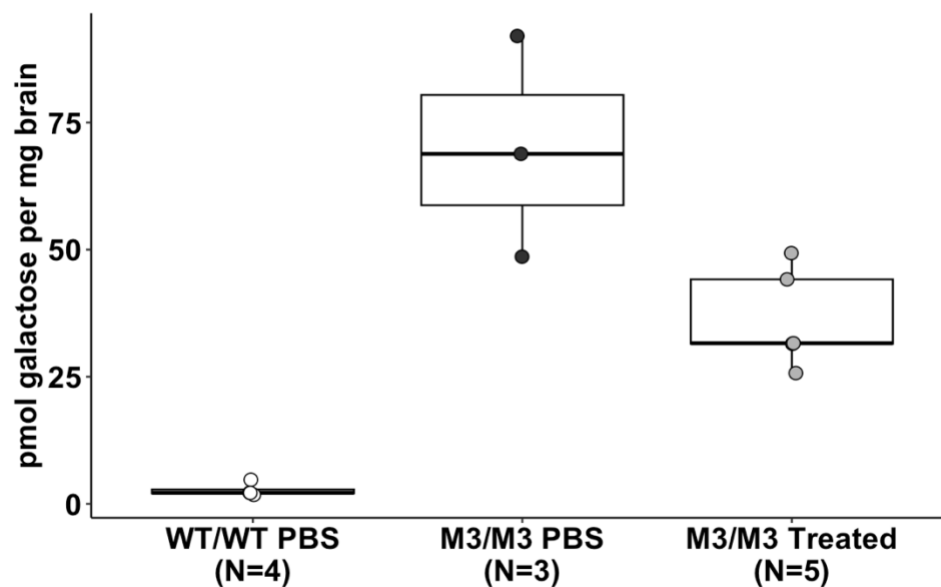


FIGURE 21. Galactose levels in brains of PBS-treated WT rats (white symbols), PBS-treated GALT-null rats (black symbols), and scAAV9-hGALT-treated GALT-null rats (gray symbols) **two months after treatment**. Pairwise comparison between M3 PBS and M3 treated group ($P = 0.071$, Wilcoxon Test).

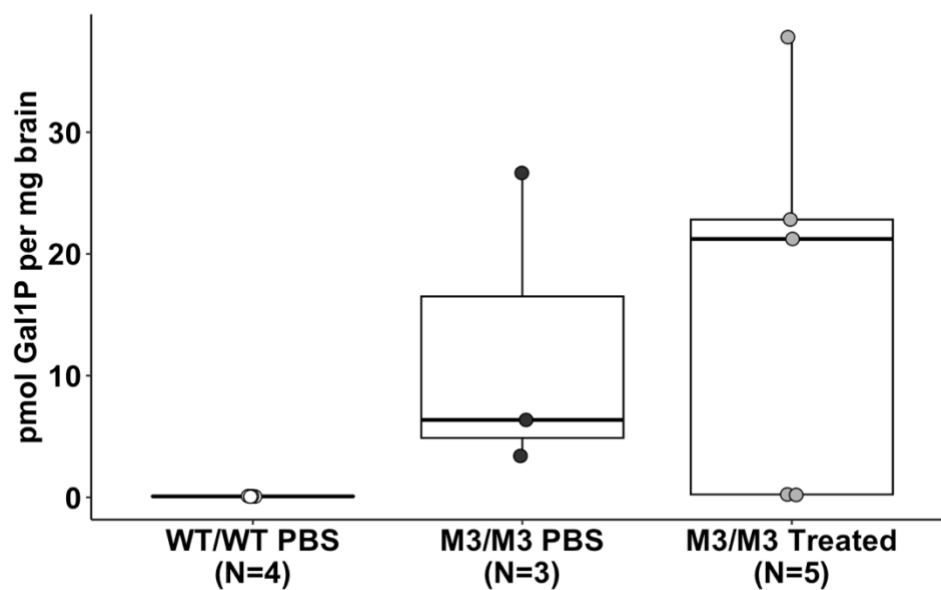


FIGURE 22. Gal1P levels in brains of PBS-treated WT rats (white symbols), PBS-treated GALT-null rats (black symbols), and scAAV9-hGALT-treated GALT-null rats (gray symbols) **two months after treatment**. Pairwise comparison between M3 PBS and M3 treated group ($P = 1.00$, Wilcoxon Test).

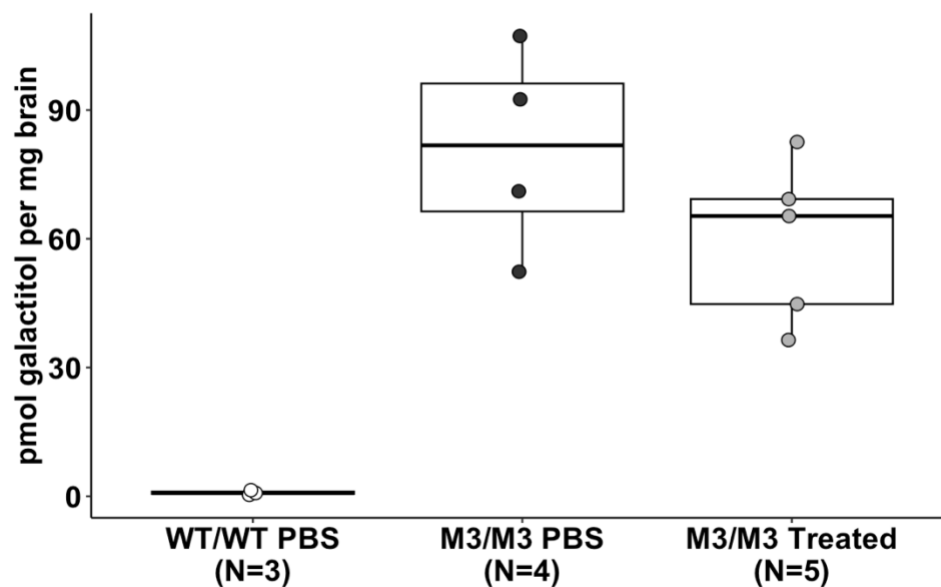


FIGURE 23. Galactitol levels in brains of PBS-treated WT rats (white symbols), PBS-treated GALT-null rats (black symbols), and scAAV9-hGALT-treated GALT-null rats (gray symbols) **four months after treatment**. Pairwise comparison between M3 PBS and M3 treated group ($P = 0.190$, Wilcoxon Test).

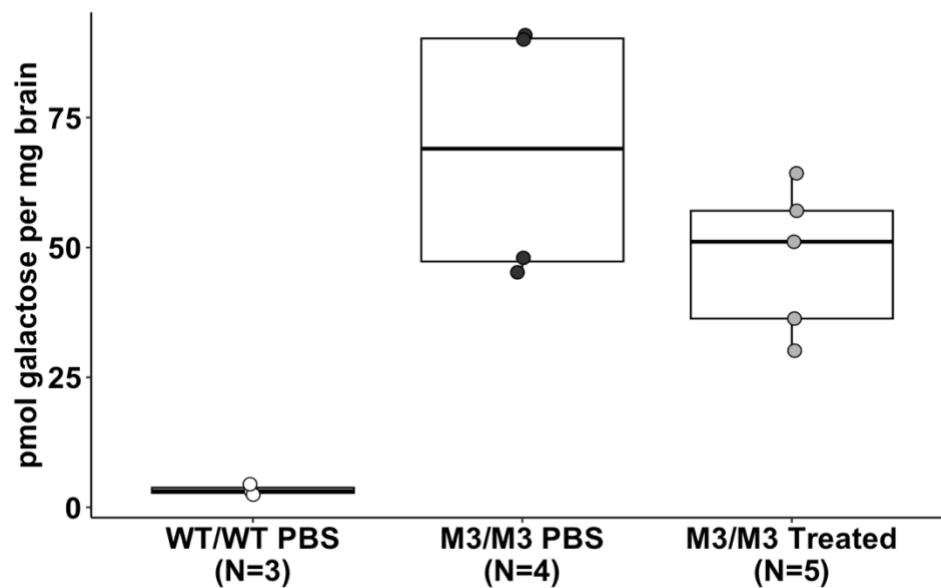


FIGURE 24. Galactose levels in brains of PBS-treated WT rats (white symbols), PBS-treated GALT-null rats (black symbols), and scAAV9-hGALT-treated GALT-null rats (gray symbols) **four months after treatment**. Pairwise comparison between M3 PBS and M3 treated group ($P = 0.413$, Wilcoxon Test).

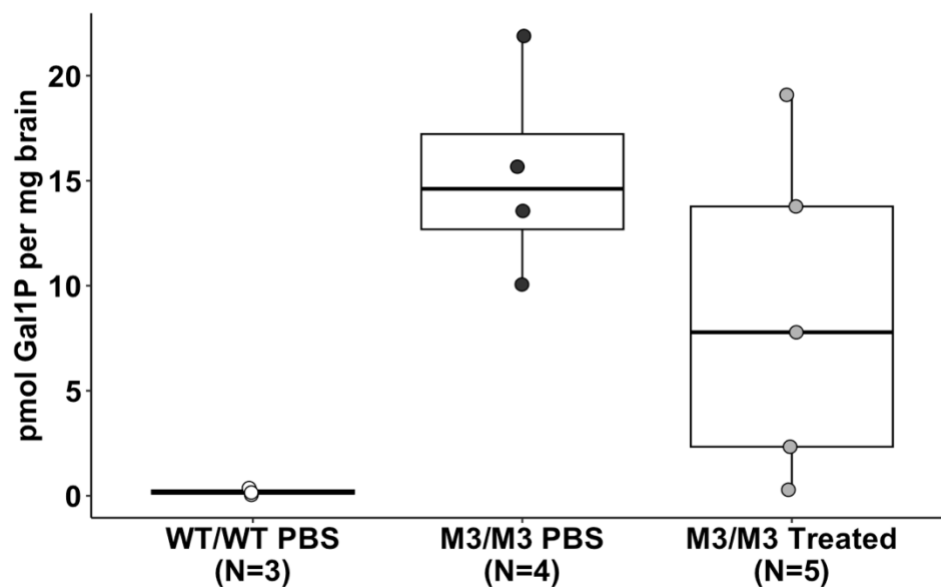


FIGURE 25. Gal1P levels in brains of PBS-treated WT rats (white symbols), PBS-treated GALT-null rats (black symbols), and sAAV9-hGALT-treated GALT-null rats (gray symbols) **four months after treatment**. Pairwise comparison between M3 PBS and M3 treated group ($P = 0.29$, Wilcoxon Test).

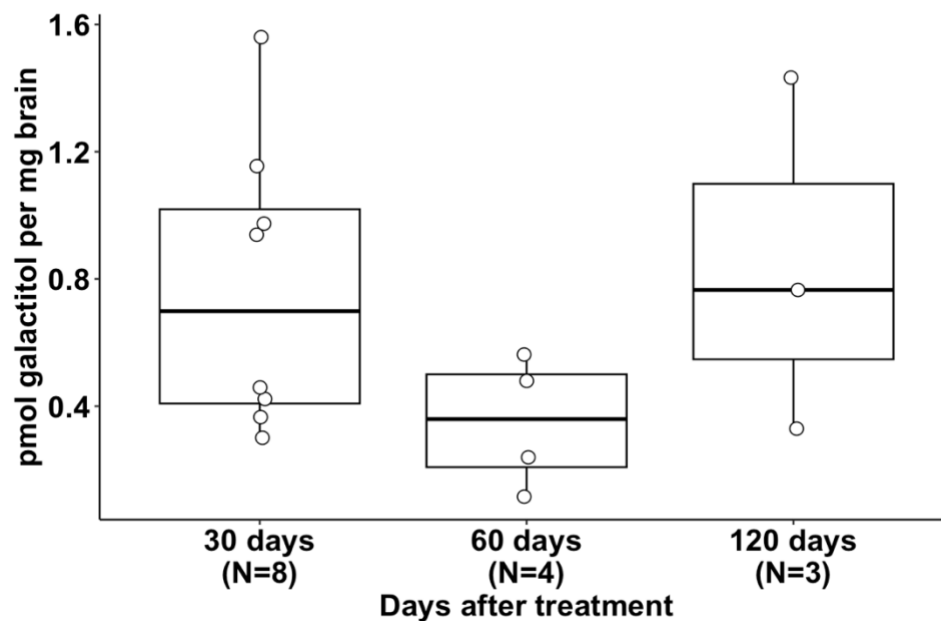


FIGURE 26. Galactitol levels over time in brains of WT rats treated with PBS. Pairwise comparisons performed between 30 and 60 days ($P = 0.34$, Wilcoxon Test), and 60 and 120 days ($P = 0.34$, Wilcoxon Test).

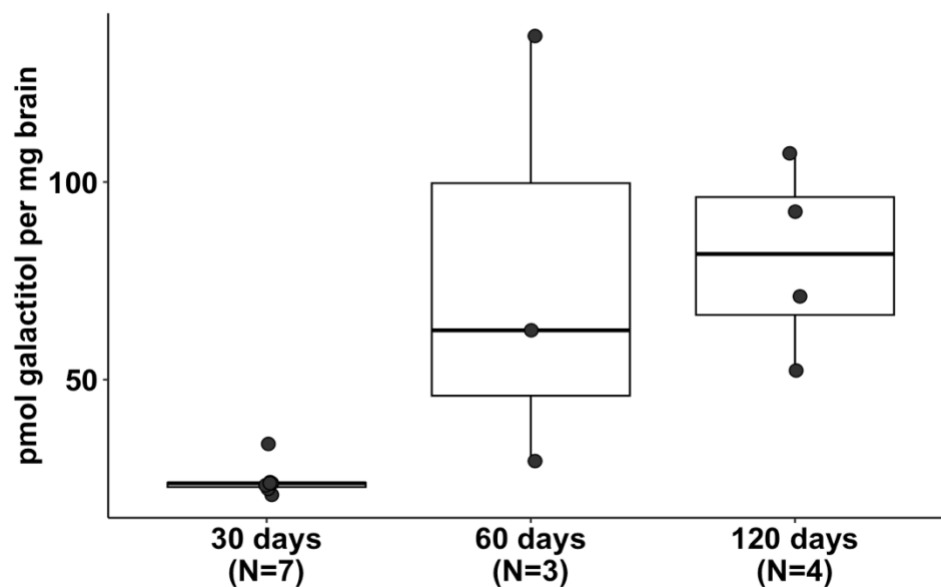


FIGURE 27. Galactitol levels over time in brains of M3/M3 rats treated with PBS. Pairwise comparisons performed between 30 and 60 days ($P = 0.05$), and 60 and 120 days ($P = 0.857$, Wilcoxon Test).

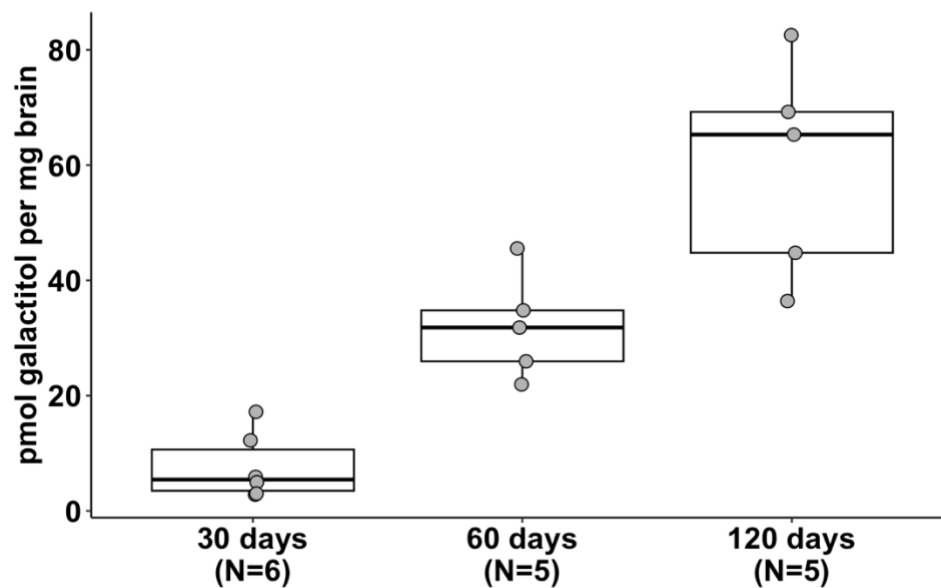


FIGURE 28. Galactitol levels over time in brains of M3/M3 rats treated with scAAV9.CBh.HA-hGALT. Pairwise comparisons performed between 30 and 60 days ($P = 0.0065$), and 60 and 120 days ($P = 0.0317$, Wilcoxon Test).

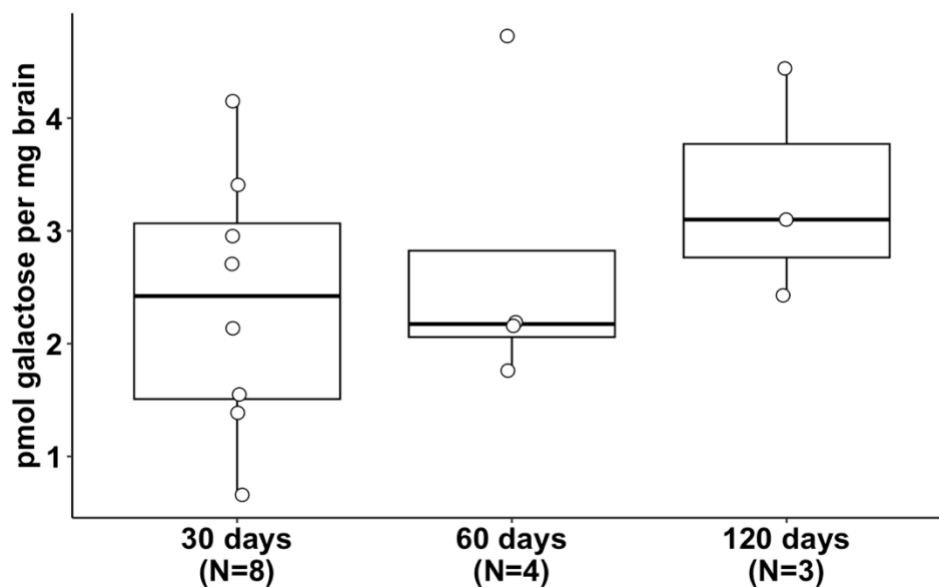


FIGURE 29. Galactose levels over time in brains of WT rats treated with PBS. Pairwise comparisons performed between 30 and 60 days ($P = 0.68$, Wilcoxon Test), and 60 and 120 days ($P = 0.60$, Wilcoxon Test).

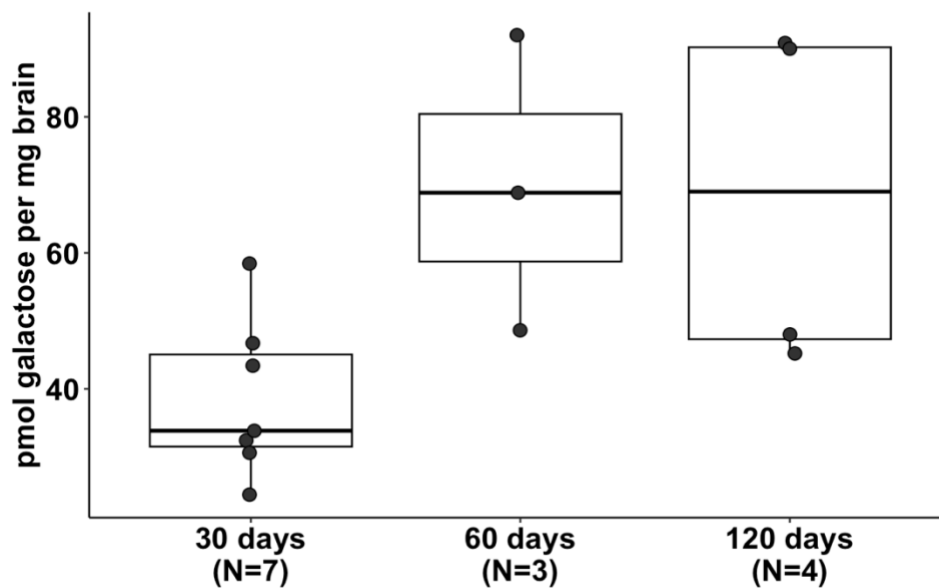


FIGURE 30. Galactose levels over time in brains of M3/M3 rats treated with PBS. Pairwise comparisons performed between 30 and 60 days ($P = 0.064$, Wilcoxon Test), and 60 and 120 days ($P = 0.629$, Wilcoxon Test).

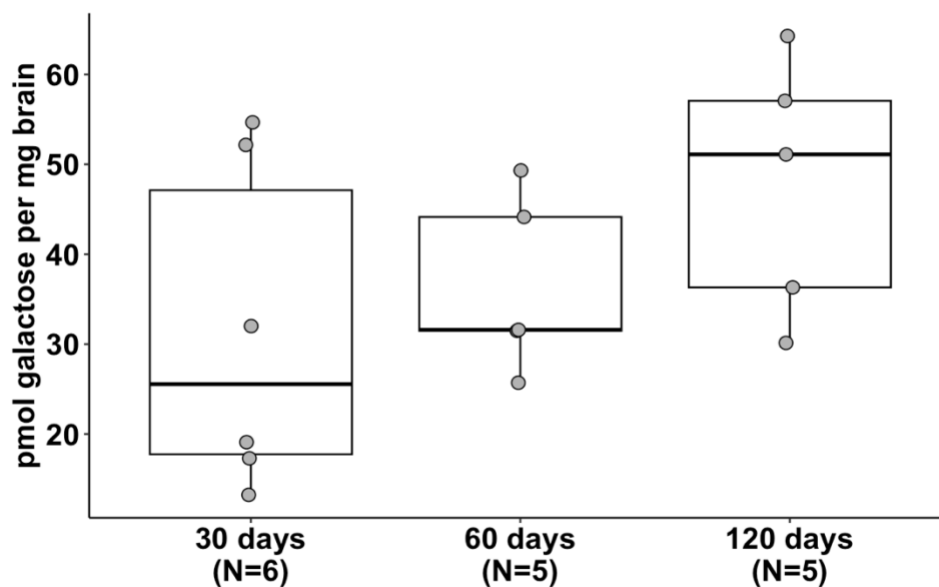


FIGURE 31. Galactose levels over time in brains of M3/M3 rats treated with scAAV9.CBh.HA-hGALT. Pairwise comparisons performed between 30 and 60 days ($P = 0.79$, Wilcoxon Test), and 60 and 120 days ($P = 0.33$, Wilcoxon Test).

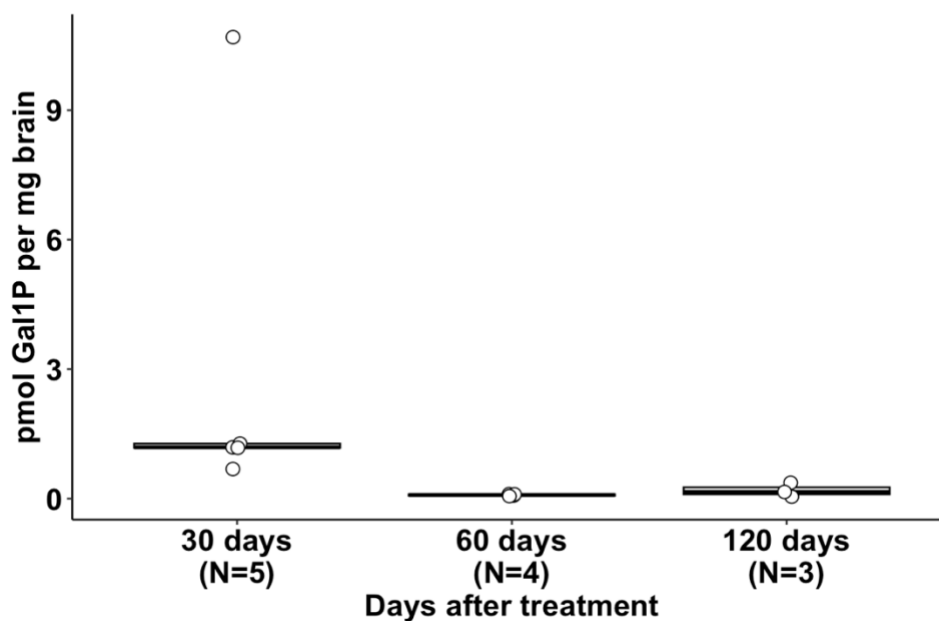


FIGURE 32. Gal1P levels over time in brains of WT rats treated with PBS. Pairwise comparisons performed between 30 and 60 days ($P = 0.048$, Wilcoxon Test), and 60 and 120 days ($P = 0.629$, Wilcoxon Test).

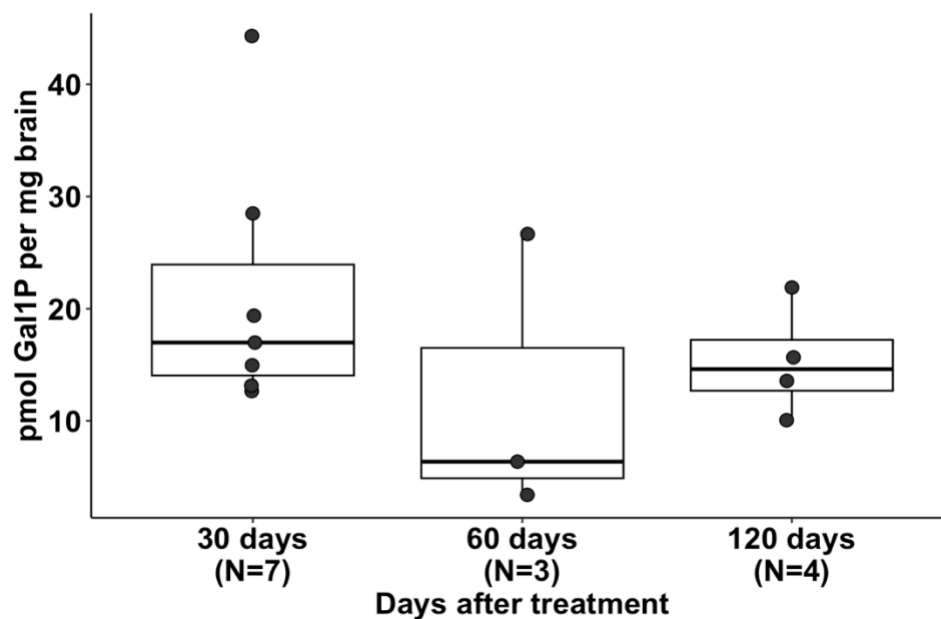


FIGURE 33. Gal1P levels over time in brains of M3/M3 rats treated with PBS. Pairwise comparisons performed between 30 and 60 days ($P = 0.63$, Wilcoxon Test), and 60 and 120 days ($P = 0.63$, Wilcoxon Test).

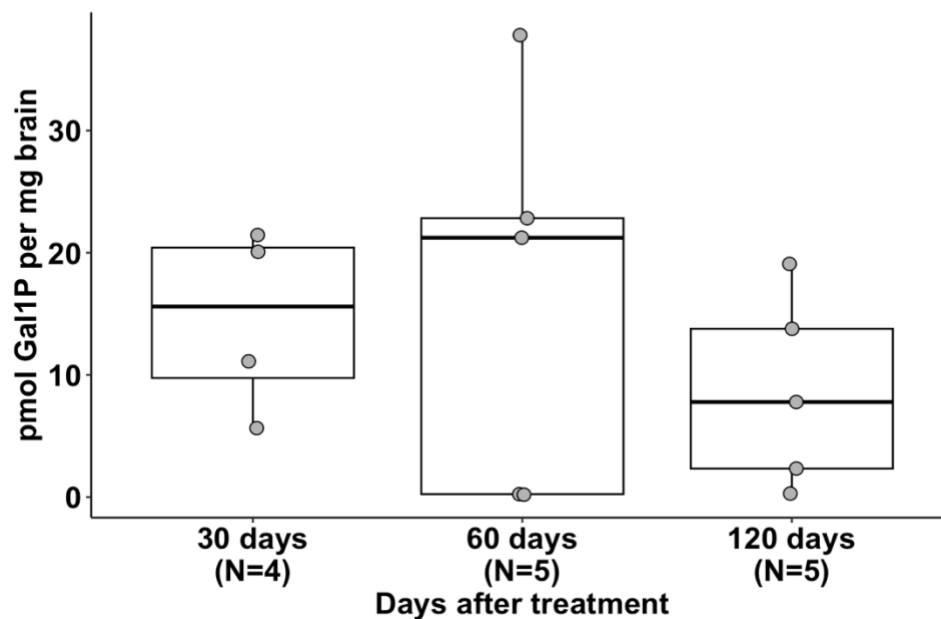


FIGURE 34. Gal1P levels over time in brains of M3/M3 rats treated with scAAV9.CBh.HA-hGALT. Pairwise comparisons performed between 30 and 60 days ($P = 0.90$, Wilcoxon Test), and 60 and 120 days ($P = 0.90$, Wilcoxon Test).

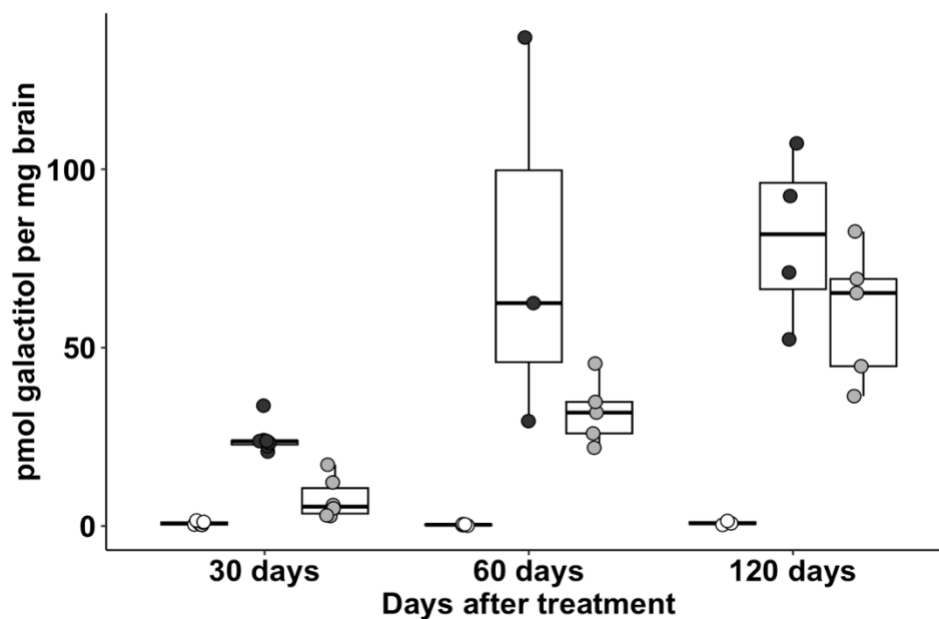


FIGURE 35. Galactitol levels over time in brains of PBS-treated WT rats (white symbols), PBS-treated GALT-null rats (black symbols), and scAAV9-hGALT-treated GALT-null rats (gray symbols).

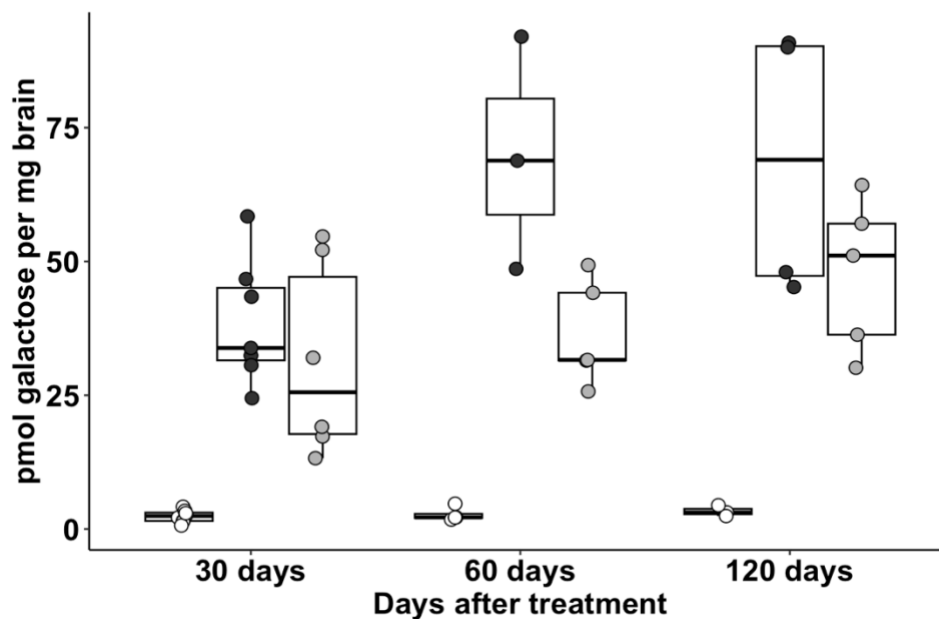


FIGURE 36. Galactose levels over time in brains of PBS-treated WT rats (white symbols), PBS-treated GALT-null rats (black symbols), and scAAV9-hGALT-treated GALT-null rats (gray symbols).

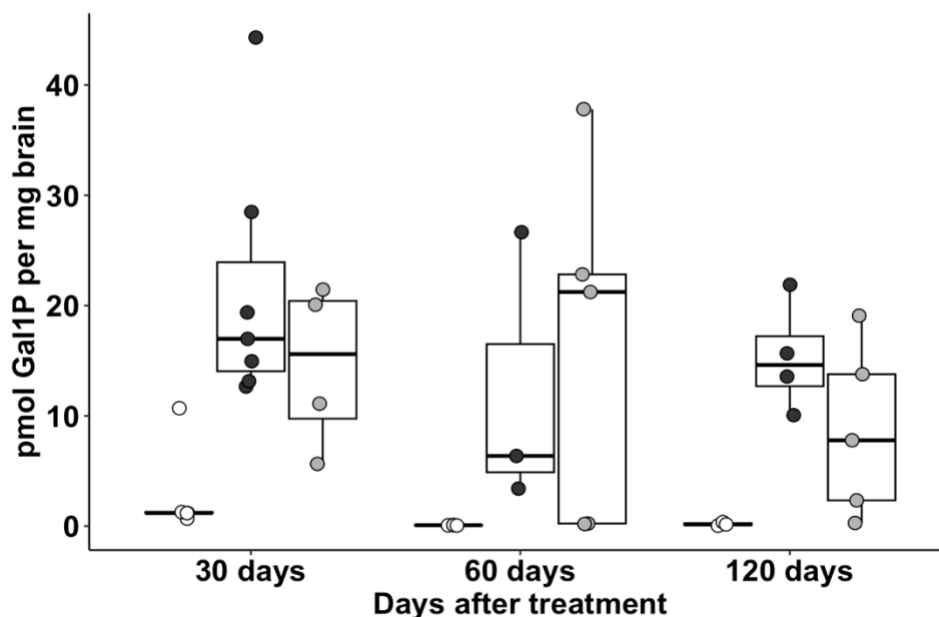


FIGURE 37. Gal1P levels over time in brains of PBS-treated WT rats (white symbols), PBS-treated GALT-null rats (black symbols), and scAAV9-hGALT-treated GALT-null rats (gray symbols).

Extent and Kinetics of Metabolic Rescue in Plasma

Galactitol levels in the plasma of M3/M3 rats treated with scAAV9.CBh.HA-hGALT showed a significant decrease 30 days after treatment compared to M3/M3 PBS treated rats (Figure 38). Galactitol levels were lowered, albeit not to the level of statistical significance, 60 and 120 days after treatment (Figures 40, 42). Galactose levels in the plasma of M3/M3 treated rats showed a downward trend without statistical significance at all timepoints (Figures 39, 41, 43). Gal1P is not detectable in plasma because it is an intracellular metabolite. Over time, galactitol levels for WT/WT rats treated with PBS decreased significantly from 30 days to 120 days after treatment (Figure 44). On the contrary, galactitol levels remained relatively constant for both M3/M3 rats treated with PBS and M3/M3 rats treated with scAAV9.CBh.HA-hGALT (Figures 46, 48). Similarly, galactose levels did not change significantly over the course of the

study for any experimental group (Figures 45, 47, 49). However, as an exception, galactitol levels did increase significantly between 60 and 120 days after treatment for the M3/M3 rats treated with scAAV9.CBh.HA-hGALT (Figure 49). Again, whether these differences are meaningful or reflect statistics of small numbers is difficult to determine from this pilot study.

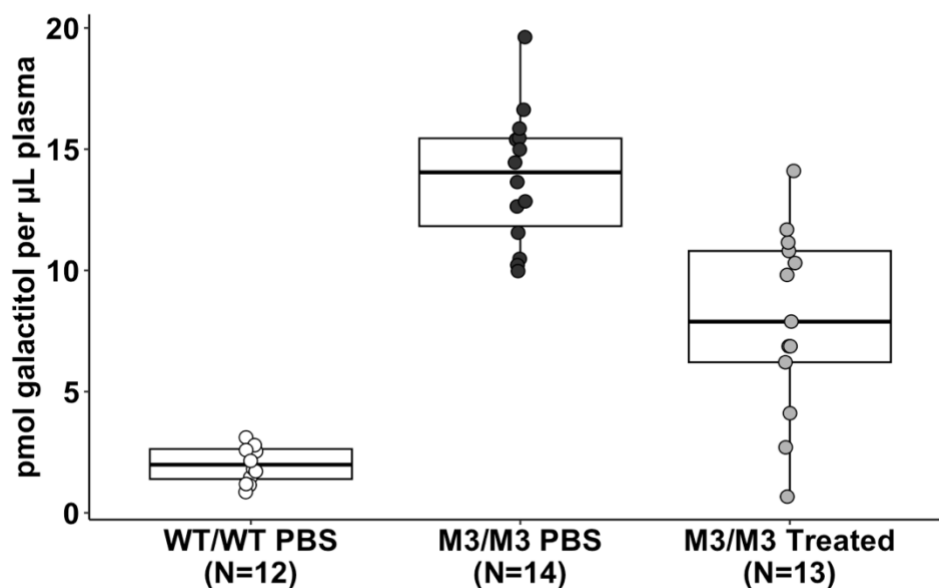


FIGURE 38. Galactitol levels in plasma of PBS-treated WT rats (white symbols), PBS-treated GALT-null rats (black symbols), and scAAV9-hGALT-treated GALT-null rats (gray symbols) **one month after treatment**. Pairwise comparison between M3 PBS and M3 treated group ($P = 0.0289$, Wilcoxon Test).

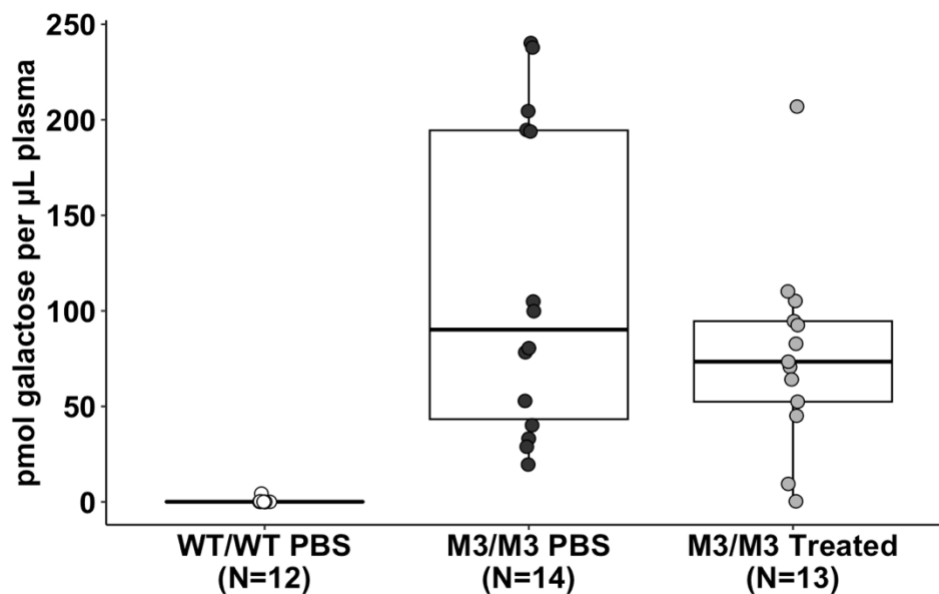


FIGURE 39. Galactose levels in plasma of PBS-treated WT rats (white symbols), PBS-treated GALT-null rats (black symbols), and scAAV9-hGALT-treated GALT-null rats (gray symbols) **one month after treatment**. Pairwise comparison between M3 PBS and M3 treated group ($P = 0.7789$, Wilcoxon Test).

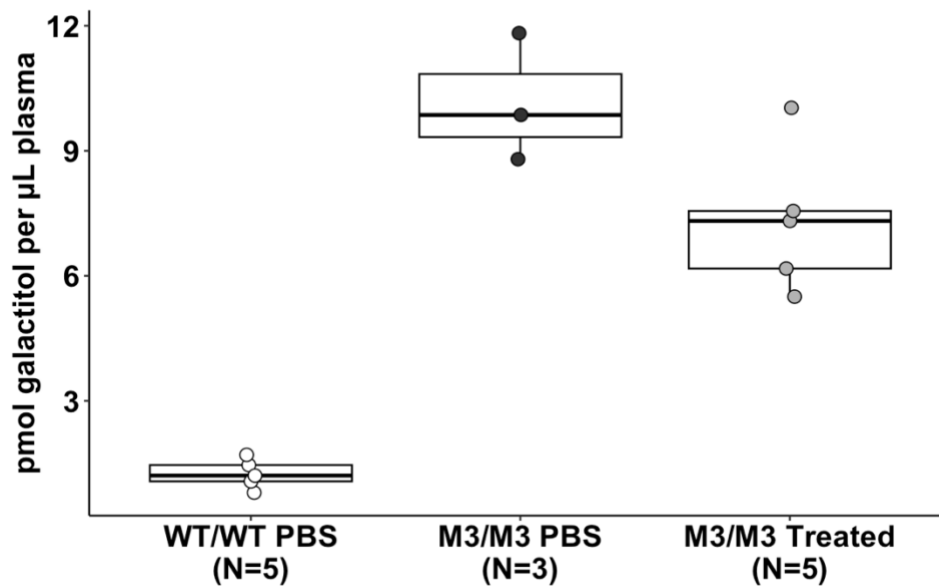


FIGURE 40. Galactitol levels in plasma of PBS-treated WT rats (white symbols), PBS-treated GALT-null rats (black symbols), and scAAV9-hGALT-treated GALT-null rats (gray symbols) **two months after treatment**. Pairwise comparison between M3 PBS and M3 treated group ($P = 0.143$, Wilcoxon Test).

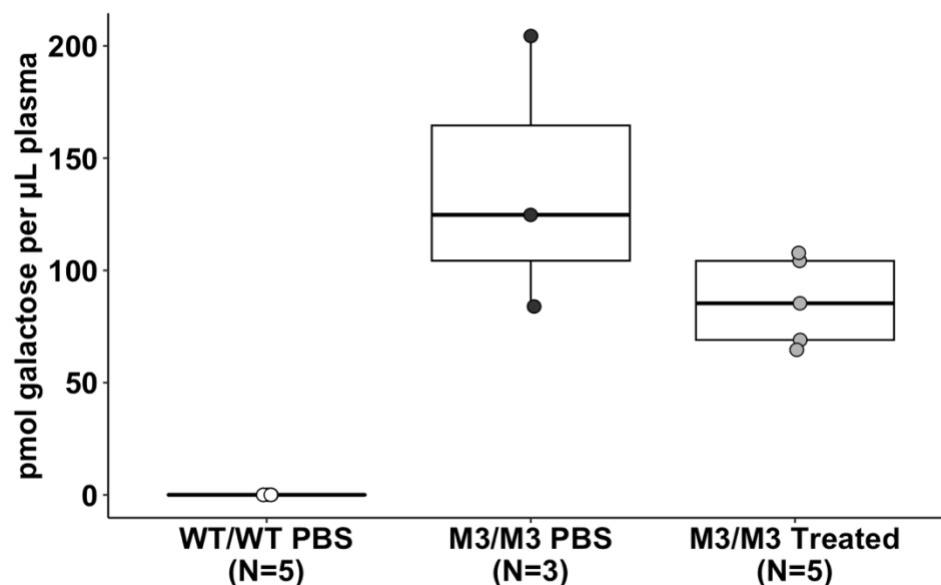


FIGURE 41. Galactose levels in plasma of PBS-treated WT rats (white symbols), PBS-treated GALT-null rats (black symbols), and scAAV9-hGALT-treated GALT-null rats (gray symbols) **two months after treatment**. Pairwise comparison between M3 PBS and M3 treated group ($P = 0.250$, Wilcoxon Test).

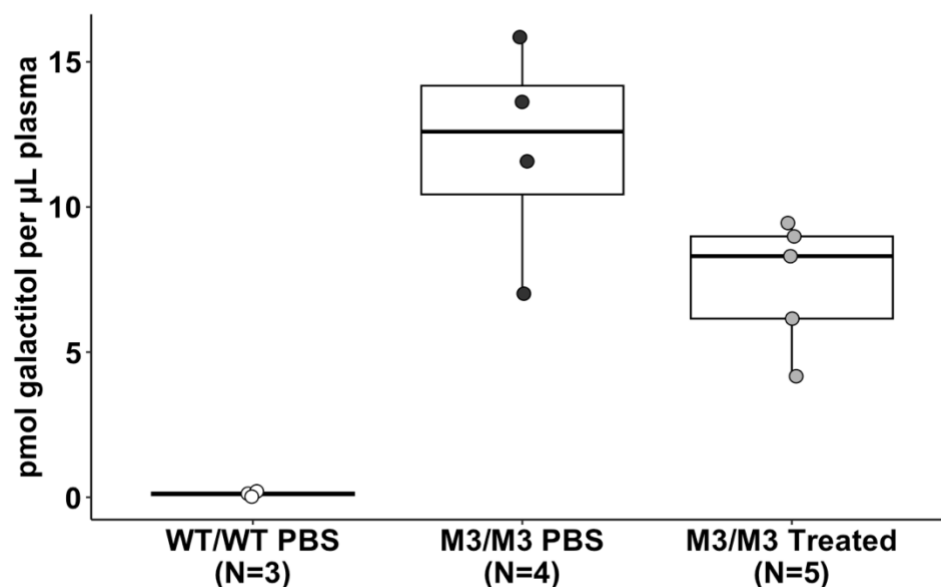


FIGURE 42. Galactitol levels in plasma of PBS-treated WT rats (white symbols), PBS-treated GALT-null rats (black symbols), and scAAV9-hGALT-treated GALT-null rats (gray symbols) **four months after treatment**. Pairwise comparison between M3 PBS and M3 treated group ($P = 0.111$, Wilcoxon Test).

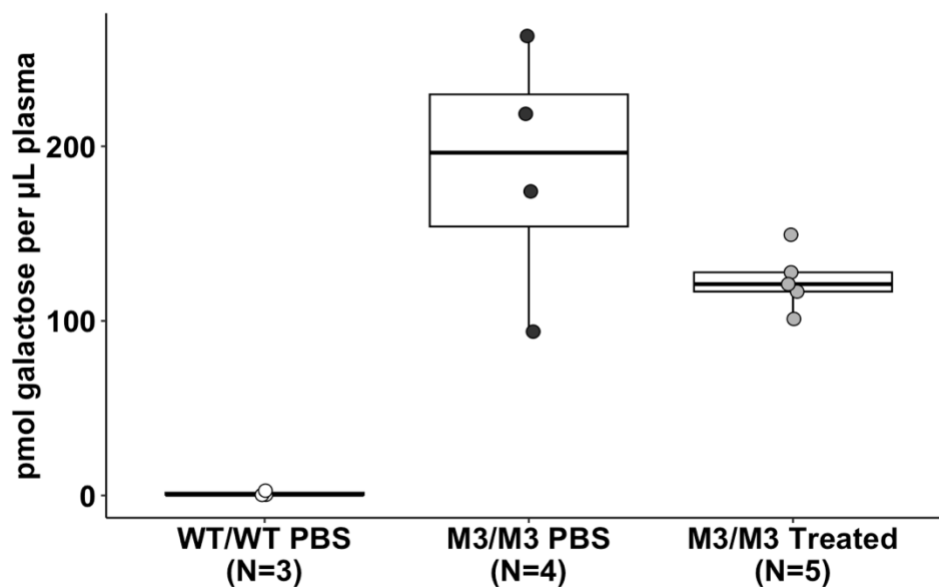


FIGURE 43. Galactose levels in plasma of PBS-treated WT rats (white symbols), PBS-treated GALT-null rats (black symbols), and scAAV9-hGALT-treated GALT-null rats (gray symbols) **four months after treatment**. Pairwise comparison between M3 PBS and M3 treated group ($P = 0.286$, Wilcoxon Test).

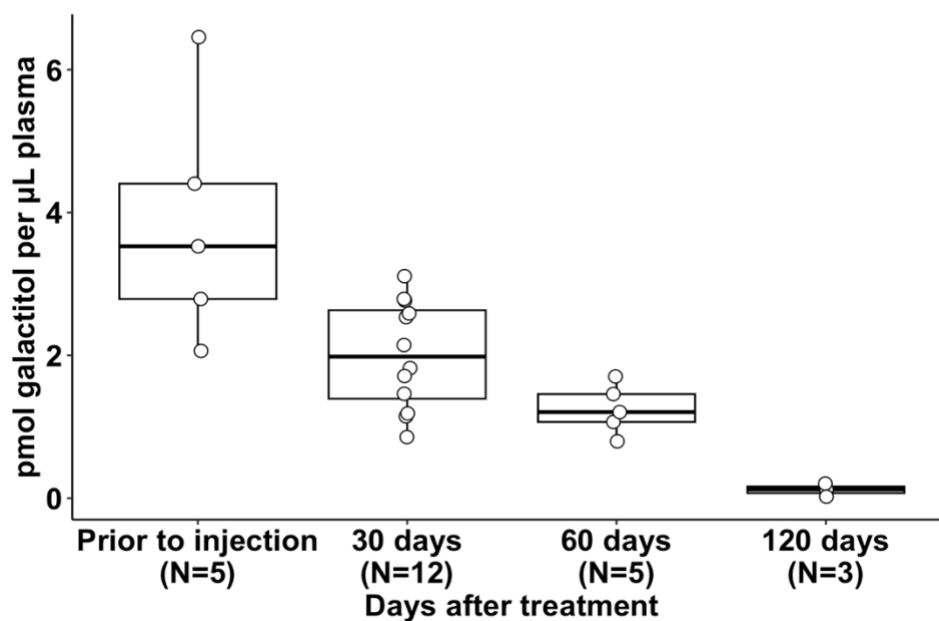


FIGURE 44. Galactitol levels over time in plasma of WT/WT rats treated with PBS. Pairwise comparisons performed between 30 and 60 days ($P = 0.048$, Wilcoxon Test), and 60 and 120 days ($P = 0.043$, Wilcoxon Test).

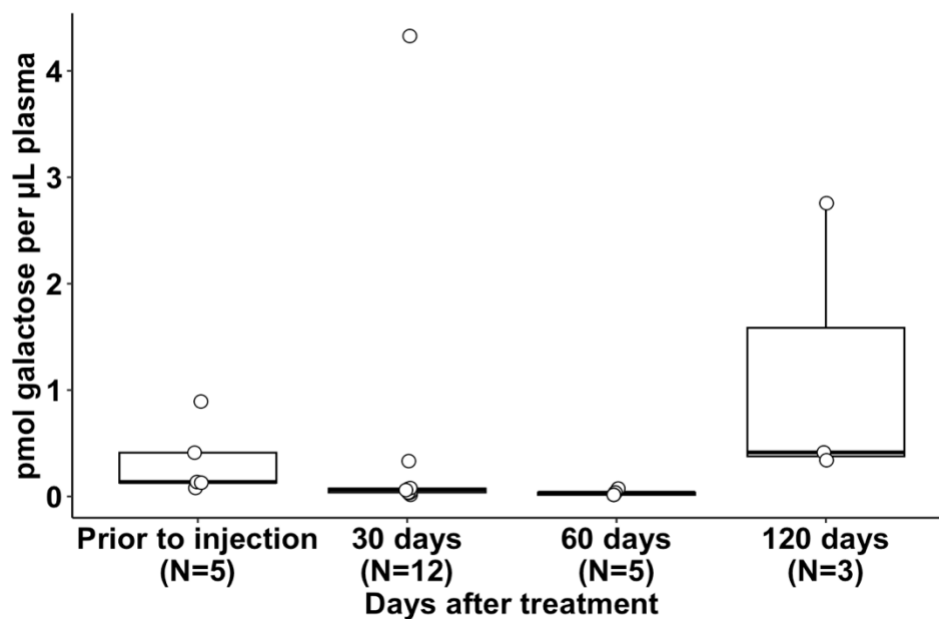


FIGURE 45. Galactose levels over time in plasma of WT/WT rats treated with PBS. Pairwise comparisons performed between 30 and 60 days ($P = 0.192$, Wilcoxon Test), and 60 and 120 days ($P = 0.054$, Wilcoxon Test).

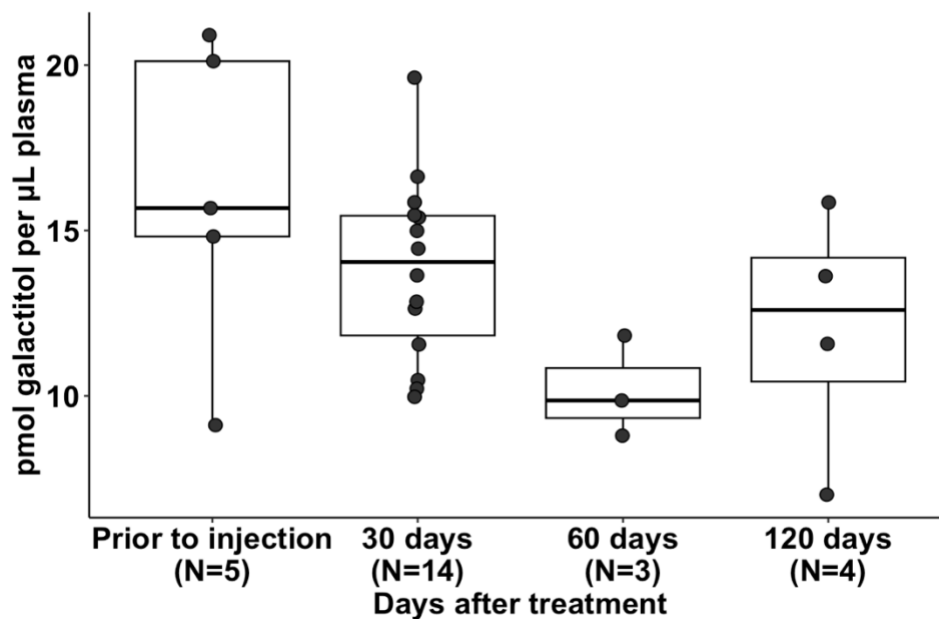


FIGURE 46. Galactitol levels over time in plasma of M3/M3 rats treated with PBS. Pairwise comparisons performed between 30 and 60 days ($P = 0.19$, Wilcoxon Test), and 60 and 120 days ($P = 0.63$, Wilcoxon Test).

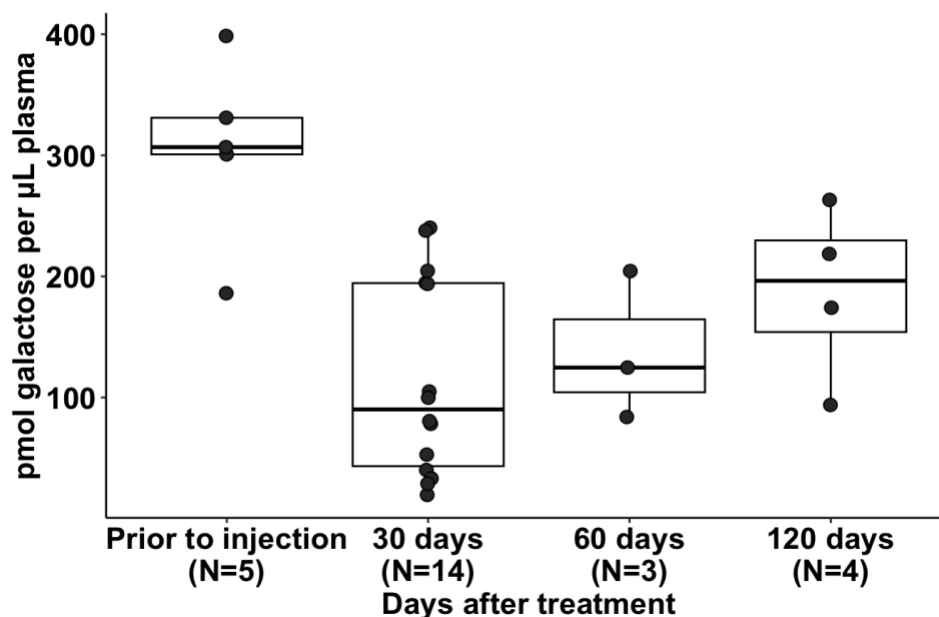


FIGURE 47. Galactose levels over time in plasma of M3/M3 rats treated with PBS. Pairwise comparisons performed between 30 and 60 days ($P = 0.51$, Wilcoxon Test), and 60 and 120 days ($P = 0.48$, Wilcoxon Test).

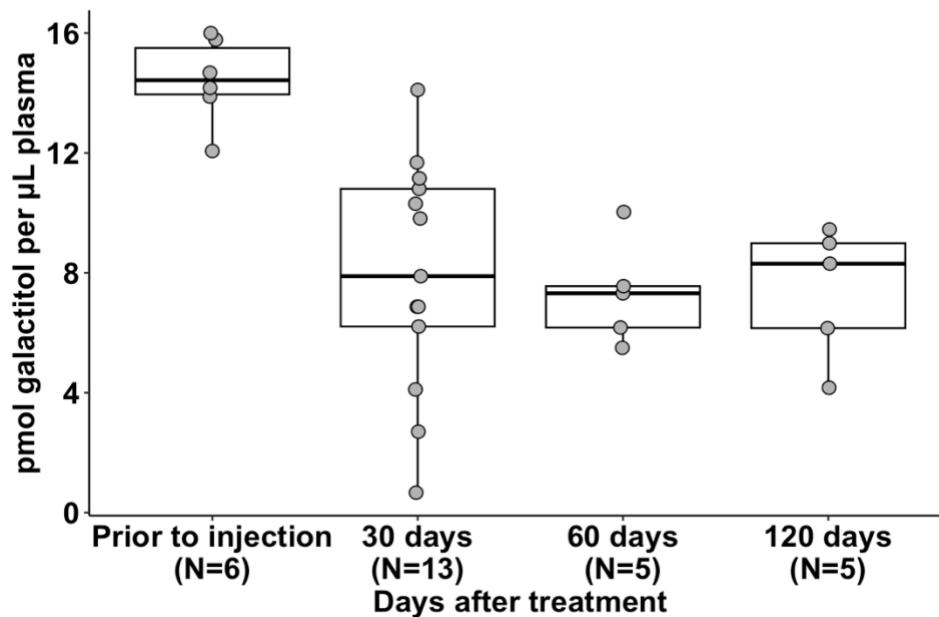


FIGURE 48. Galactitol levels over time in plasma of M3/M3 rats treated with scAAV9.CBh.HA-hGALT. Pairwise comparisons performed between 30 and 60 days ($P = 0.7597$, Wilcoxon Test), and 60 and 120 days ($P = 1.00$, Wilcoxon Test).

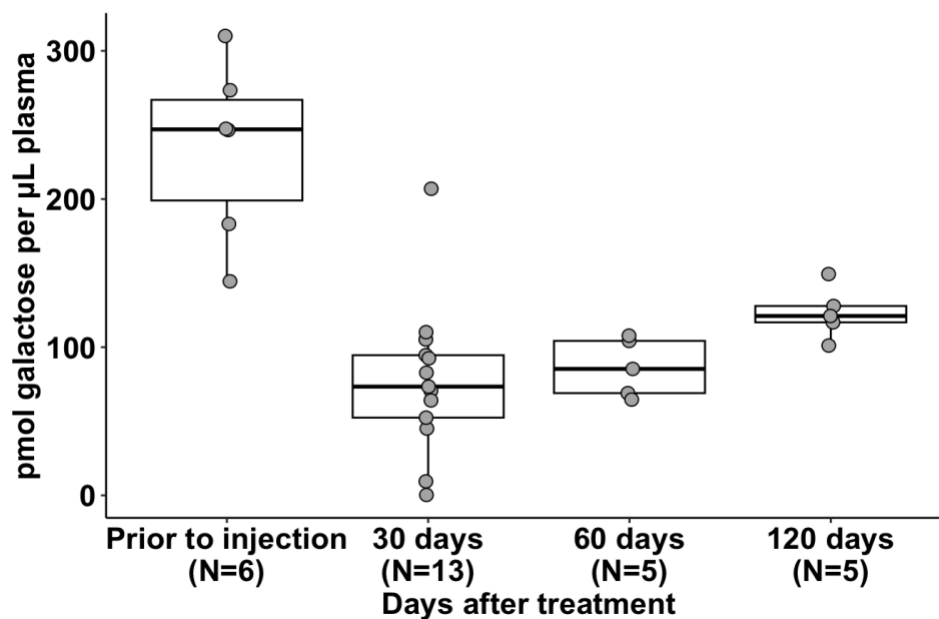


FIGURE 49. Galactose levels over time in plasma of M3/M3 rats treated with scAAV9.CBh.hGALT. Pairwise comparisons performed between 30 and 60 days ($P = 0.5663$, Wilcoxon Test), and 60 and 120 days ($P = 0.038$, Wilcoxon Test).

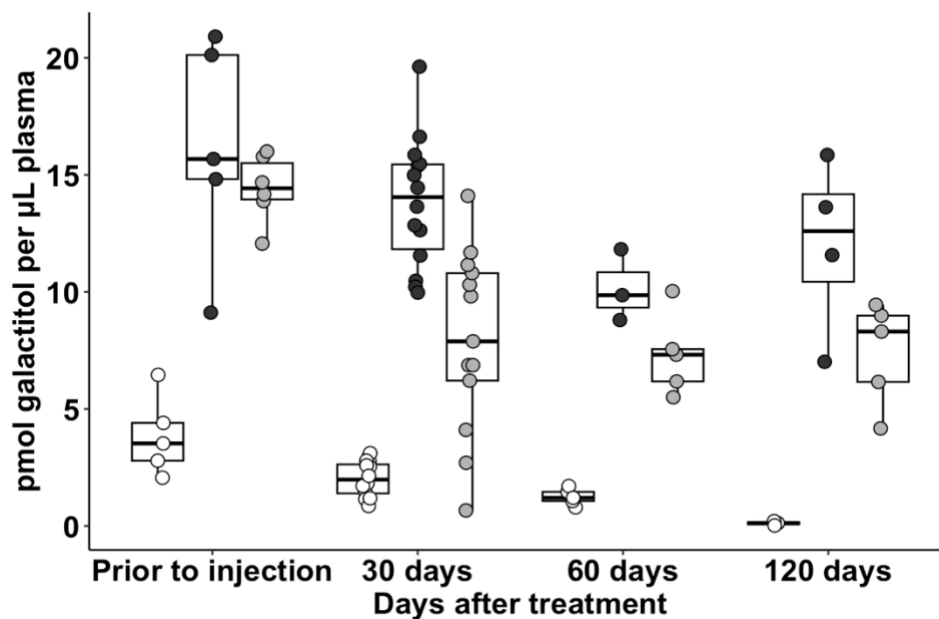


FIGURE 50. Galactitol levels over time in plasma of PBS-treated WT rats (white symbols), PBS-treated GALT-null rats (black symbols), and scAAV9-hGALT-treated GALT-null rats (gray symbols).

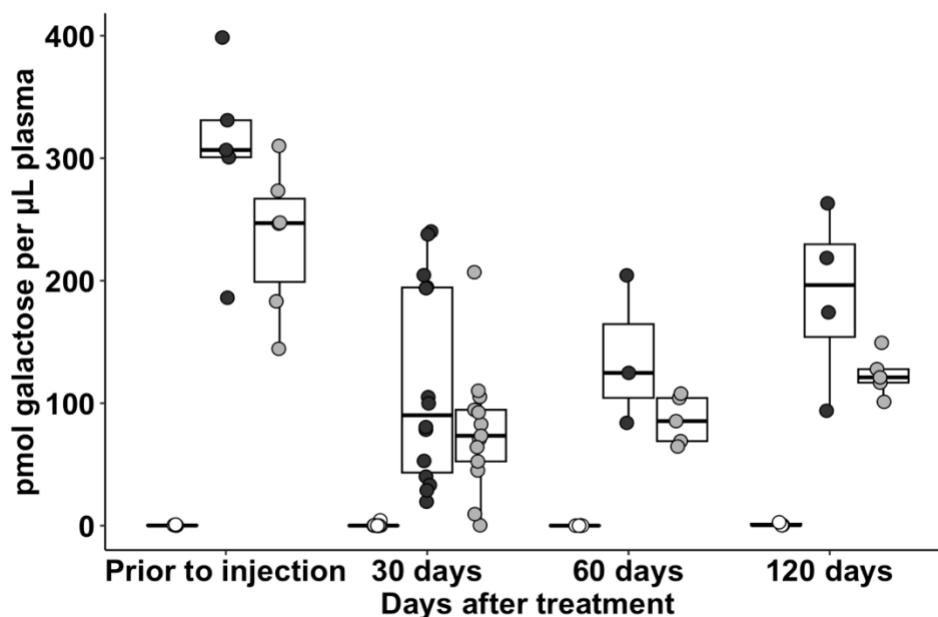


FIGURE 51. Galactose levels over time in plasma of PBS-treated WT rats (white symbols), PBS-treated GALT-null rats (black symbols), and scAAV9-hGALT-treated GALT-null rats (gray symbols).

Association between brain GALT activity and metabolite levels

Galactitol, galactose, and Gal1P levels in brain weakly negatively correlated with brain GALT activity (Figures 52-54). However, the precipitous drop in metabolite levels with GALT activity indicates that even low amounts of GALT activity may be sufficient to reduce metabolic toxicity. Similarly, plasma galactose was weakly negatively correlated with brain GALT activity (Figure 56), while plasma galactitol displayed a moderate negative correlation (Figure 55). This apparent negative relationship between plasma metabolites and brain GALT activity may be indicative of the potential role of brain GALT in nullifying metabolic toxicity in the blood.

* For FIGURES 52-56, rats harvested 30 days after treatment are represented by circles, 60 days after treatment are represented by squares, and 120 days after treatment are represented by triangles.

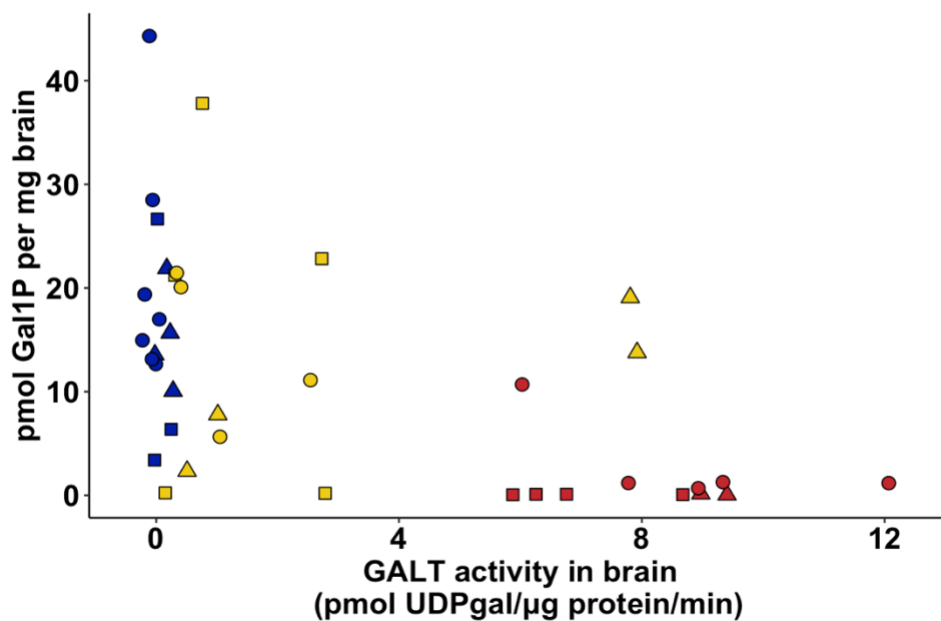


FIGURE 54. Relationship between brain Gal1P levels and brain GALT activity in PBS-treated WT rats (red symbols), PBS-treated GALT-null rats (blue symbols), and scAAV9-hGALT-treated GALT-null rats (yellow symbols).

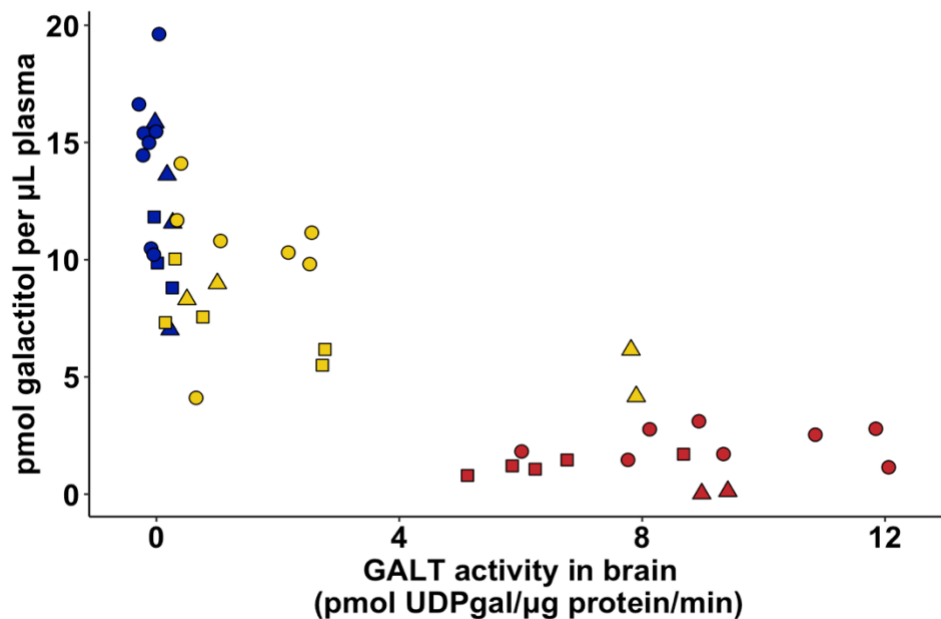


FIGURE 55. Relationship between plasma galactitol levels and brain GALT activity in PBS-treated WT rats (red symbols), PBS-treated GALT-null rats (blue symbols), and scAAV9-hGALT-treated GALT-null rats (yellow symbols).

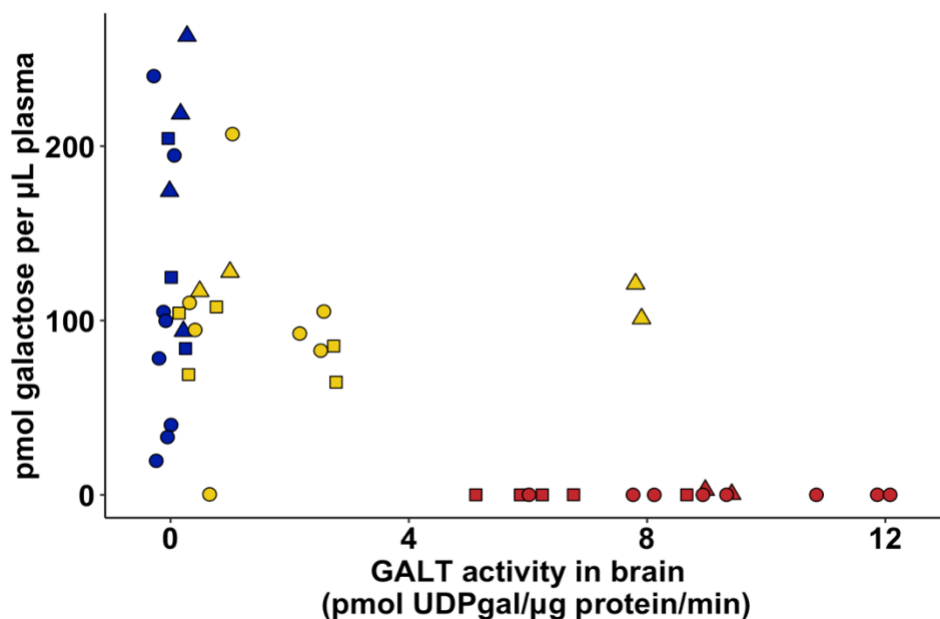


FIGURE 56. Relationship between plasma galactose levels and brain GALT activity in PBS-treated WT rats (red symbols), PBS-treated GALT-null rats (blue symbols), and scAAV9-hGALT-treated GALT-null rats (yellow symbols).

Discussion

These data demonstrated that we achieved partial metabolic correction in the brain and plasma, mostly at earlier ages after treatment. Galactitol appeared to respond most effectively to the treatment compared to galactose and Gal1P (Figures 35-37, 50, 51). The galactitol levels were significantly reduced in M3/M3 rat brains treated with scAAV9.CBh.HA-hGALT 30 days after treatment (Figure 17). Likewise, the plasma galactitol levels were significantly reduced 30 days after treatment as well (Figure 38). On the contrary, galactose and Gal1P levels stayed relatively constant and comparable to M3/M3 rats treated with PBS in both the brain and plasma. We can postulate that the correction of Gal1P was challenging primarily because of its charged state and strictly intracellular localization. Because galactose and galactitol can cross the plasma membrane transduced cells can help metabolize the galactose and galactitol from their non-

transduced neighboring cells, but Gal1P remains cell autonomous due to its inability to cross the cell membrane. However, it is unclear why galactitol responded better than galactose since both molecules are plasma soluble and capable of crossing the blood-brain barrier (BBB). If the brain were the primary site of galactose metabolism in these M3/M3 treated rats due to a trace amount of GALT activity, the differential correction of metabolites could have been a function of differential permeabilities of galactitol and galactose in the BBB caused by factors such as alterations in transporters, enzymes, and receptor proteins in the BBB. Similarly, limited metabolic efficacy in the plasma despite a lack of detectable liver and muscle GALT activity suggests that the brain may be capable of correcting metabolic toxicity systemically. Alternatively, there may have been GALT activity in tissues that were not tested contributing to the effects in the plasma.

Furthermore, GALT activity assays of brain homogenate confirmed effective transduction of scAAV9.CBh.HA-hGALT in the brain, these results did not address whether GALT was selectively or ubiquitously restored in different parts of the brain and/or different cell types. We are currently working on immunohistochemistry and double-label immunofluorescence to answer these questions, but we were unable to gather the needed data for this project due to time constraints. Nonetheless, the weak correlations between brain GALT activity and brain metabolites could be a result of differential transduction of the number of cells in the brain (Figures 52-54). For example, a lower number of cells might need to transduce in a homogenate to detect GALT activity, but a larger number of cells might be required to reduce metabolite accumulation. Further research is needed to clarify the findings.

Chapter 4: Discussion, Limitations and Future Directions

General Discussion

CG is a potentially lethal autosomal recessive disorder caused by a severe deficiency of the GALT enzyme [1]. The current standard of care for patients with galactosemia is a galactose-restricted diet, which can nullify acute neonatal complications but is inadequate in preventing long-term complications. Even patients who follow a strict galactose-restricted diet can suffer from profound long-term effects on the central nervous system, possibly due to chronic intoxication with endogenously produced galactose combined with cell dysfunction due to metabolic derangement. One promising treatment option being investigated for CG is *GALT* gene therapy, which aims to restore GALT activity directly. Based on the clinical data from biochemical variants of galactosemia like DG, restoring GALT activity up to 25% might be sufficient to rescue clinical phenotypes of the disease. Even patients with only trace GALT activity show generally milder outcomes [43].

The first aim of this study was to test whether we can express the hGALT transgene using a scAAV9 vector administered intrathecally. We wanted to restore GALT activity in the brain particularly due to the brain-related phenotypes in older patients with CG. Overall, we were able to restore notable GALT activity in the brain and sustain it over four months. Since GALT activity was undetectable in the liver and muscle at all time points, this study design can be used to investigate the phenotypes that can be rescued with predominantly brain GALT restoration rather than hepatocytes that primarily metabolize galactose in the body. To be clear, undetectable GALT activity in the liver and muscle at the time points tested does not necessarily mean that no tissues other than brain expressed hGALT at any time point. Other tissues and time points will need to be studied to clarify this point.

Previous studies have suggested accumulation of galactose metabolites from the Leloir pathway may be the root cause of some of the adverse phenotypes associated with CG [1, 6, 10, 12]. Hence, the second aim of this study was to measure the functional efficacy of GALT restoration in brain in terms of metabolite levels in the brain and plasma. We could not achieve complete rescue of any of the metabolites at most time points in both brain and plasma. Galactitol responded well at 30 days after treatment in both the brain and plasma. Although the metabolite levels were trending downwards, we could not significantly reduce the metabolic abnormality at the three timepoints in the study. The lack of significant metabolic efficacy could be attributed to insufficient GALT restoration in the brain and/or the inability of the brain to metabolize galactose sufficiently to “scrub the blood”. Given that we did see trends in the data suggestive that at least some metabolites were improved by the treatment, it is also possible analyzing additional samples will bring clarity. Although our current findings are inconclusive, future research, for example with higher doses or altered virus with improved access to the brain could potentially provide greater metabolic impact.

Limitations

One of the most important limitations of this project was the inconsistencies associated with using a viral vector in the CNS. Starting from the production process, vector preparations do not produce identical particles with variations in capsids and impurities. Different lots from the same core facility have shown significant variations in their transduction and penetrating efficiencies [44]. In addition to the production of viral vectors, IT injections could have also contributed to the large variability in the treated rats. Unfortunately, there is no objective measure to assess the quality of the injection to ensure that all of the treatment was injected in

the subarachnoid space of the spinal cord with limited leakage into the surrounding tissue. This can alter the number of viral genomes effectively administered to each GALT-null animal, and in turn, affect the transduction efficiency and GALT restoration. Moreover, even though the animal was held in the Trendelenburg position for 30 minutes after the surgery, this may not have been sufficient to move most of the vector from the spinal cord to the brain. Our pilot analysis of the spinal cord revealed significant GALT activity in the spinal cords of treated GALT-null rats, specifically in the cervical section of the spinal column (data not shown). This result indicates that a significant amount of administered virus may have been sequestered in the spinal cord and never reached the brain [45]. However, IHC and other experiments need to be conducted to test this hypothesis and assess the vector biodistribution.

Another major limitation of this study was the small number of samples analyzed for each group because of the pilot nature of this project. Due to small cohort sizes, we were unable to test behavioral phenotypes such as the balance beam and Morris water maze to study the phenotypic efficacy of the GALT restoration we did achieve in GALT-null rats described here.

Future Directions

Beyond the scope of this pilot study, we plan to test larger cohorts in order to account for biological variation between our outbred rats, and to enable meaningful tests of behavioral efficacy. To be clear, we do not know how much GALT is required in the brain to improve phenotypic outcomes. Another possible area of future research is increasing the dosage of the virus administered. Since we did not observe any overt evidence of toxicity in our animals, and used a considerably lower dosage compared to other animal studies, we would be interested in testing whether we can achieve better GALT restoration in the brain with a higher dose, and if

that might allow improved normalization of metabolites in the brain and plasma. In addition to the brain and liver, we have collected muscle, heart, spleen, lungs, kidneys, and spinal cords from all the animals in the study. We would like to measure the GALT activity in these other tissues as well as metabolite levels to understand the holistic effects of IT virus administration in GALT-null rats.

We can also consider weaning treated and control pups to a lower galactose chow in order to more closely mimic the galactose-restricted diet of humans with CG. Finally, we can try treating adult rats rather than adolescents. The goal of such studies would be to ask whether adverse long-term outcomes might be reversible. While much work remains to be done, the results reported here represent a major conceptual step in the direction of developing an effective gene therapy treatment option for adolescent patients with CG.

References

1. Berry, G., *Classic Galactosemia and Clinical Variant Galactosemia*, in *GeneReviews® [Internet]*, E.D. Adam MP, Mirzaa GM, et al., Editor. 2020, University of Washington: Seattle (WA).
2. Leslie, N.D., et al., *The Human Galactose-1-phosphate Uridyl Transferase Gene*. *Genomics*, 1992. **14**: p. 474-480.
3. Dobrowolski, S.F., et al., *Analysis of common mutations in the galactose-1-phosphate uridyl transferase gene: new assays to increase the sensitivity and specificity of newborn screening for galactosemia*. *J Mol Diagn*, 2003. **5**(1): p. 42-7.
4. Elsevier, J.P. and J.L. Fridovich-Keil, *The Q188R mutation in human galactose-1-phosphate uridylyltransferase acts as a partial dominant negative*. *Journal of Biological Chemistry*, 1996. **271**(50): p. 32002-32007.
5. Ficicioglu, C., et al., *Duarte (DG) galactosemia: a pilot study of biochemical and neurodevelopmental assessment in children detected by newborn screening*. *Mol Genet Metab*, 2008. **95**(4): p. 206-12.
6. Demirbas, D., et al., *The ability of an LC-MS/MS-based erythrocyte GALT enzyme assay to predict the phenotype in subjects with GALT deficiency*. *Mol Genet Metab*, 2019. **126**(4): p. 368-376.
7. Fridovich-Keil, J. and J. Walter, *Galactosemia*, in *The Online Metabolic & Molecular Bases of Inherited Disease*, D. Valle, et al., Editors. 2008, McGraw Hill. p. <http://www.ommbid.com/>.
8. Rubio-Gozalbo, M.E., et al., *The natural history of classic galactosemia: lessons from the GalNet registry*. *Orphanet J Rare Dis*, 2019. **14**(1): p. 86.
9. Fridovich-Keil, J.L. and G.T. Berry, *Pathophysiology of long-term complications in classic galactosemia: What we do and do not know*. *Mol Genet Metab*, 2022. **137**(1-2): p. 33-39.
10. Huttenlocher, P.R., R.E. Hillman, and Y.E. Hsia, *Pseudotumor cerebri in galactosemia*. *The Journal of Pediatrics*, 1970. **76**(6): p. 902-905.
11. Waggoner, D.D., N.R. Buist, and G.N. Donnell, *Long-term prognosis in galactosaemia: results of a survey of 350 cases*. *J Inher Metab Dis*, 1990. **13**(6): p. 802-18.

12. Koch, T.K., et al., *Neurologic complications in galactosemia*. *Pediatr Neurol*, 1992. **8**(3): p. 217-20.
13. Nelson, M.D., Jr., et al., *Galactosemia: evaluation with MR imaging*. *Radiology*, 1992. **184**(1): p. 255-61.
14. Welsink-Karssies, M.M., et al., *Gray and white matter are both affected in classical galactosemia: An explorative study on the association between neuroimaging and clinical outcome*. *Molecular Genetics and Metabolism*, 2020. **131**(4): p. 370-379.
15. Holden, H.M., I. Rayment, and J.B. Thoden, *Structure and function of enzymes of the Leloir pathway for galactose metabolism*. *J Biol Chem*, 2003. **278**(45): p. 43885-8.
16. Daenzer, J.M.I. and J.L. Fridovich-Keil, *Chapter Twelve - Drosophila melanogaster Models of Galactosemia*, in *Current Topics in Developmental Biology*, L. Pick, Editor. 2017, Academic Press. p. 377-395.
17. Sørensen, M., et al., *Hepatic galactose metabolism quantified in humans using 2-18F-fluoro-2-deoxy-D-galactose PET/CT*. *Journal of nuclear medicine : official publication, Society of Nuclear Medicine*, 2011. **52**(10): p. 1566-1572.
18. Berry, G.T., et al., *The Rate of Endogenous Galactose Synthesis in Normals and Patients with Galactose-1-Phosphate Uridyltransferase Deficiency 704*. *Pediatric Research*, 1998. **43**(4): p. 122-122.
19. Berry, G.T., et al., *Endogenous Synthesis of Galactose in Normal Men and Patients with Hereditary Galactosemia*. *Lancet*, 1995. **346**(8982): p. 1073-1074.
20. Berry, G.T., et al., *The rate of de novo galactose synthesis in patients with galactose-1-phosphate uridyltransferase deficiency*. *Mol Genet Metab*, 2004. **81**(1): p. 22-30.
21. Schadewaldt, P., et al., *Age dependence of endogenous galactose formation in Q188R homozygous galactosemic patients*. *Mol Genet Metab*, 2004. **81**(1): p. 31-44.
22. Walter, J.H. and J.L. Fridovich-Keil, *Galactosemia*, in *The Online Metabolic and Molecular Bases of Inherited Disease*, D.L. Valle, et al., Editors. 2019, McGraw-Hill Education: New York, NY.
23. Bulcha, J.T., et al., *Viral vector platforms within the gene therapy landscape*. *Signal Transduction and Targeted Therapy*, 2021. **6**(1): p. 53.
24. Belur, L.R., et al., *Comparative Effectiveness of Intracerebroventricular, Intrathecal, and Intranasal Routes of AAV9 Vector Administration for Genetic Therapy of Neurologic*

- Disease in Murine Mucopolysaccharidosis Type I*. *Frontiers in Molecular Neuroscience*, 2021. **14**.
25. Bailey, R.M., et al., *Development of Intrathecal AAV9 Gene Therapy for Giant Axonal Neuropathy*. *Molecular Therapy - Methods & Clinical Development*, 2018. **9**: p. 160-171.
 26. Cabrera-Salazar, M.A., et al., *Timing of therapeutic intervention determines functional and survival outcomes in a mouse model of late infantile batten disease*. *Mol Ther*, 2007. **15**(10): p. 1782-8.
 27. Sondhi, D., et al., *Survival advantage of neonatal CNS gene transfer for late infantile neuronal ceroid lipofuscinosis*. *Exp Neurol*, 2008. **213**(1): p. 18-27.
 28. Naso, M.F., et al., *Adeno-Associated Virus (AAV) as a Vector for Gene Therapy*. *BioDrugs*, 2017. **31**(4): p. 317-334.
 29. Zhang, H., et al., *Several rAAV vectors efficiently cross the blood-brain barrier and transduce neurons and astrocytes in the neonatal mouse central nervous system*. *Mol Ther*, 2011. **19**(8): p. 1440-8.
 30. Li, C. and R.J. Samulski, *Engineering adeno-associated virus vectors for gene therapy*. *Nature Reviews Genetics*, 2020. **21**(4): p. 255-272.
 31. SA, R., et al., *A Galactose-1-phosphate Uridyltransferase-Null Rat Model of Classic Galactosemia Mimics Relevant Patient Outcomes and Reveals Tissue-Specific and Longitudinal Differences in Galactose Metabolism*. *J Inherit Metab Dis*, 2020. **43**(3): p. 518-528.
 32. Rasmussen, S.A., J.M.I. Daenzer, and J.L. Fridovich-Keil, *A pilot study of neonatal GALT gene replacement using AAV9 dramatically lowers galactose metabolites in blood, liver, and brain and minimizes cataracts in GALT-null rat pups*. *J Inherit Metab Dis*, 2021. **44**(1): p. 272-281.
 33. Daenzer, J.M.I., et al., *Neonatal GALT gene replacement offers metabolic and phenotypic correction through early adulthood in a rat model of classic galactosemia*. *J Inherit Metab Dis*, 2022. **45**(2): p. 203-214.
 34. Delnoy, B., A.I. Coelho, and M.E. Rubio-Gozalbo, *Current and Future Treatments for Classic Galactosemia*. *J Pers Med*, 2021. **11**(2).
 35. Sanders, R.D., et al., *UDP-galactose 4' epimerase (GALE) is essential for development of Drosophila melanogaster*. *Dis Model Mech*, 2010. **3**(9-10): p. 628-38.

36. Haynes, W., *Benjamini–Hochberg Method*, in *Encyclopedia of Systems Biology*, W. Dubitzky, et al., Editors. 2013, Springer New York: New York, NY. p. 78-78.
37. Ohno, K., et al., *Kinetics and MR-Based Monitoring of AAV9 Vector Delivery into Cerebrospinal Fluid of Nonhuman Primates*. *Molecular Therapy - Methods & Clinical Development*, 2019. **13**: p. 47-54.
38. Wolff, J.A., et al., *Direct Gene Transfer into Mouse Muscle in Vivo*. *Science*, 1990. **247**(4949): p. 1465-1468.
39. Rasmussen, S.A., et al., *A galactose-1-phosphate uridylyltransferase-null rat model of classic galactosemia mimics relevant patient outcomes and reveals tissue-specific and longitudinal differences in galactose metabolism*. *J Inherit Metab Dis*, 2020. **43**(3): p. 518-528.
40. Sapcariu, S.C., et al., *Simultaneous extraction of proteins and metabolites from cells in culture*. *MethodsX*, 2014. **1**: p. 74-80.
41. Ross, K.L., C.N. Davis, and J.L. Fridovich-Keil, *Differential roles of the Leloir pathway enzymes and metabolites in defining galactose sensitivity in yeast*. *Mol Genet Metab*, 2004. **83**(1-2): p. 103-16.
42. van Weeghel, M., et al., *Profiling of intracellular metabolites produced from galactose and its potential for galactosemia research*. *Orphanet Journal of Rare Diseases*, 2018. **13**(1): p. 146.
43. Katler, Q.S., et al., *A multinational study of acute and long-term outcomes of Type 1 galactosemia patients who carry the S135L (c.404C > T) variant of GALT*. *J Inherit Metab Dis*, 2022.
44. O'Connor, D.M., et al., *Lot-to-Lot Variation in Adeno-Associated Virus Serotype 9 (AAV9) Preparations*. *Human Gene Therapy Methods*, 2019. **30**(6): p. 214-225.
45. Chandran, J., et al., *Assessment of AAV9 distribution and transduction in rats after administration through Intrastratial, Intracisterna magna and Lumbar Intrathecal routes*. *Gene Therapy*, 2023. **30**(1): p. 132-141.